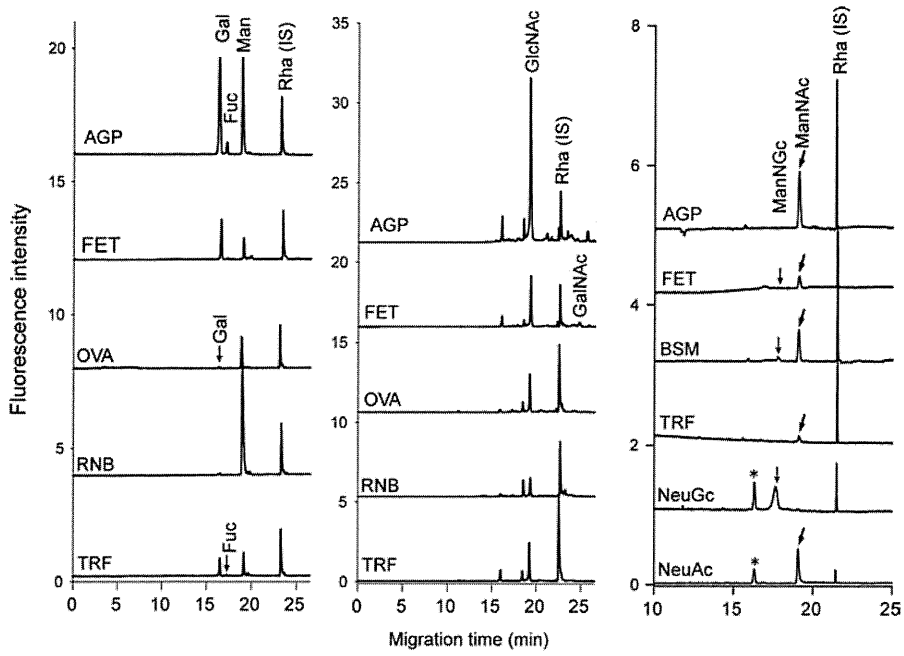

Figure 4. Analysis of component monosaccharides in hydrolysates of various glycoproteins. Analytical conditions were the same as those used for Fig. 1B. ManNGc and ManNAc were derived from NeuGc and NeuAc, respectively. AGPa = α_1-acid glycoprotein, FET = fetuin, OVA = ovalbumin, RNB = ribonuclease B, TRF = transferrin.

Table 1. Estimated content (%) of monosaccharides in various glycoprotein specimens

Glycoprotein	Man[a)]	Gal[a)]	GlcNAc[a)]	GalNAc[a)]	NeuAc[b)]	NeuGc[b)]	Fuc[a)]
α_1-Acid glycoprotein (human)	5.80	8.99	13.88	N.D.	10.02	N.D.	0.47
	5.50	7.60	13.20	N.D.	10.90	N.D.	0.70
Fetuin (bovine)	1.60	3.15	4.26	1.30	6.28	0.68	0.04
	2.45	3.49	2.62	0.54	4.62	–	0.03
Transferrin (human)	1.15	0.76	1.27	N.D.	0.91	N.D.	0.07
	1.08	1.00	1.79	0.05	1.40	N.D.	
Submaxillary mucin (bovine)	–	–	–	–	5.80	4.59	–
	–	–	–	–	1.69	1.25	
Ovalbumin (hen)	2.47	0.11	1.63	N.D.	N.D.	N.D.	N.D.
	2.80	0.12	0.28	N.D.	N.D.	N.D.	N.D.
Ribonuclease B (bovine)	4.63	N.D.	1.09	N.D.	N.D.	N.D.	N.D.
	2.20	N.D.	0.91	N.D.	N.D.	N.D.	N.D.

Values appearing on the lower line for each glycoprotein indicate reference values. N.D.: not detected; –: not determined.
a) Ref. [30].
b) Ref. [15].

reliability of quantitation for saccharides in glycoconjugate samples. Our data may therefore be more reliable than that from previously reported methods and, moreover, the sensitivity is far superior to previous methods.

3.4 Analysis of oligosaccharides in glycoproteins

The resolution of AMC-labeled oligosaccharides was evaluated using a series of α1,6-linked glucose oligomers called isomaltooligosaccharides, which had DPs distributed from 1 to 20 or more. Boric acid forms a stable complex with the linear polyalcohol structure at linear monosaccharide residues linked to AMC and the binding ability of borate to ring-formed monosaccharide residues is not high. They migrated in the order of increasing DP because of the low mobility of oligosaccharides due to the low binding capability to borate ions. To enhance the apparent mobility of AMC–oligosaccharides, we chose 250 mM potassium borate buffer (pH 9.0). As shown in Fig. 5A, they were completely resolved and oligosaccharides corresponding to DPs of more than 20 were detected within 60 min. Most *N*-linked oligosaccharides in glycoproteins are distributed between DPs of 7 and 20, which indicate that it is possible to separate a neutral oligosaccharide mixture of glycoproteins by this mode.

The separation conditions were applied to the analysis of AMC-labeled *N*-linked oligosaccharides from transferrin, fetuin, and ribonuclease B. However, the separation of acidic oligosaccharides derived from transferrin and fetuin indicates finer resolution using a somewhat lower pH of borate

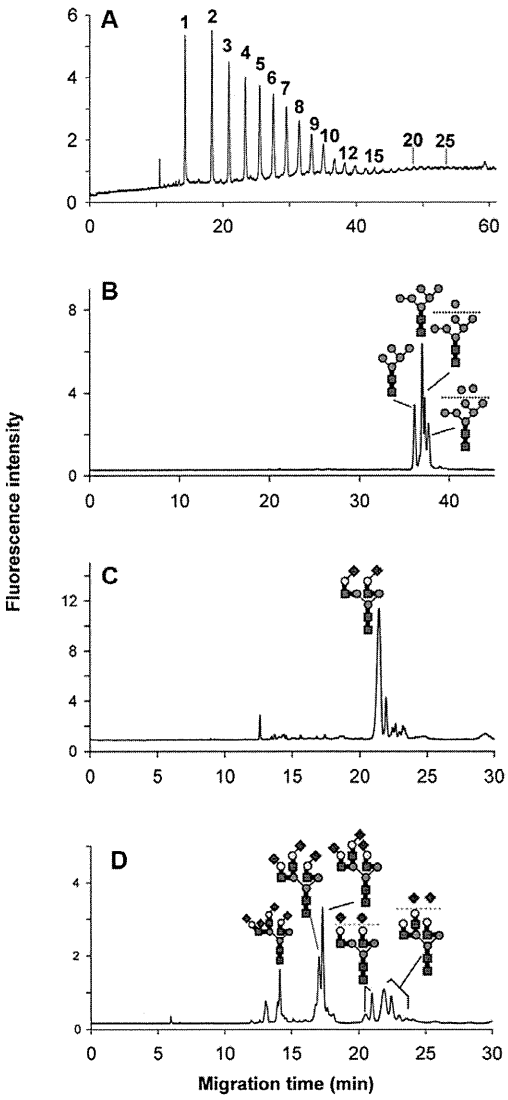

Figure 5. Separation of a mixture of isomaltooligosaccharides (A), ribonuclease B (B), transferrin (C), and fetuin (D). BGE, 1:9, v/v, mixture of ACN and borate buffer containing 0.5% hydroxypropylcellulose; 250 mM potassium borate (pH 9.0) for (A) and (B), and 100 mM Tris borate (pH 8.5) for (C) and (D), respectively.

buffer. Therefore, we applied 100 mM Tris borate (pH 8.5) for acidic oligosaccharide separation and 250 mM potassium borate buffer (pH 9.0) for neutral oligosaccharides. Results are shown in Fig. 5B–D. Oligosaccharide structures in each peak indicate there was identification based on co-migration of an AMC-oligosaccharide pool prepared by HPLC fractionation [14].

RNB contains a series of high-mannose type oligosaccharides. Their separation profile (Fig. 5B) indicates they migrated in order of their size, Man_5 to Man_9. However the separation mode could not separate linkage isomers of Man_7 and Man_8 high-mannose type oligosaccharides.

Oligosaccharides of transferrin (Fig. 5C) are mainly composed from disialylated biantennary oligosaccharides, which appeared as a large peak at 20.5 min. The subsequent small peaks should be assigned to fucosylated biantennary oligosaccharides.

Fetuin mainly contains a series of di-, tri-, and tetrasialylated triantennary glycans with variation in the linkage isomers of neuraminic acids and the presence of the Lewis X-type branch in the α1,4-linked Gal–GlcNAc branch. As shown in Fig. 5D, AMC oligosaccharides from fetuin were mainly separated according to the number of sialic acids and were further resolved by the linkage type and position as well as differences in the lactosamine linkage. The peaks detected at 14, 17, and 20–22 min correspond to tetra-, tri-, and disialylated oligosaccharides. Furthermore, four peaks appearing at 20–22 min correspond to biantennary and triantennary di-sialylated oligosaccharides. Di-sialylated triantennary oligosaccharides may be generated from partial loss of a sialic acid from triantennary oligosaccharides, which causes numerous linkage isomers and appeared as a broad peak at 22 min. Unfortunately, this separation mode is not suitable for the resolution of these oligosaccharide isomers.

3.5 Application to the separation of saccharides using other labels

Finally, as a practical test, monosaccharide mixtures and isomaltooligosaccharides were labeled with AMAC and ABEE, and the derivatives were subjected to separation with borate complex mode CE, as shown in Figs. 5A and 1B, respectively. As shown in Fig. 6, AMAC- and ABEE-labeled saccharides showed an essentially identical pattern to AMC saccharides and were also free from interference by excess reagents. ABEE derivatives migrated faster than those of AMAC derivatives so the resolution of AMAC–oligosaccharides was high. The resolution of the Glc and GlcNAc pair was achieved using ABEE derivatives. We also evaluated these separation conditions for other labels, such as *p*-aminobenzonitrile (ABN) and 5-amino-1-naphthol (AN). However, the reaction products of isomaltooligosaccharides and ABN showed an intense, unknown signal at ca. 5 min, and that of AN showed an unknown peak at 15 min (data not shown). We speculate that these peaks may be due to the products of degradation of reagents, generated during derivatization reactions.

4 Concluding remarks

A combination of alkaline borate buffer and a neutrally coated capillary enables specific determination of AMC-labeled oligosaccharides, and an LED-based fluorimetric detection was applied to sub-amol level detection of saccharides. This method enables analysis without removal of excess reagents from the reaction mixture, enabling reliable quantitative analysis of monosaccharides in hydrolysates of several glycoproteins. This separation mode is also applicable to oligosaccharides that are released from glycoproteins. The separation conditions are also applicable to other labeled saccharides. Therefore, our methods are applicable to most

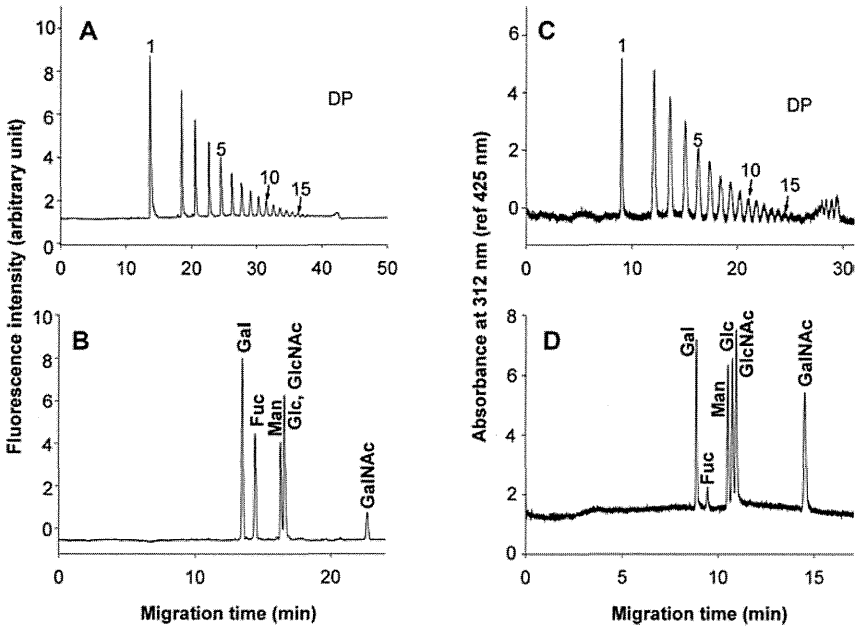

Figure 6. Application to the separation of isomaltooligosaccharides and monosaccharide mixtures labeled with AMAC (A, B) and ABEE (C, D). Analytical conditions for (A) and (C) were the same as those for Fig. 3 (A, B), while those for (B) and (D) were the same as those for Fig. 1 (B). AMAC derivatives were detected at 488 (ex)/522 (em) nm. ABEE derivatives were monitored by absorption at 210 nm.

reductively aminated saccharides, using neutral or basic labeling dyes without interference by excess reagents.

This work was supported by a Grant-in-Aid for Scientific Research (C) from the Japan Society for the Promotion of Science (JSPS), Japan, 2007–2011.

The authors have declared no conflict of interest.

5 References

[1] Anumula, K. R., *Anal. Biochem.* 2006, *350*, 1–23.

[2] Harvey, D. J., *J. Chromatogr.* 2011, *B 879*, 1196–1225.

[3] Vanderschaeghe, D., Festjens, N., Delanghe, J., Callewaert, N., *Biol. Chem.* 2010, *391*, 149–161.

[4] Briggs, J. B., Keck, R. G., Ma, S., Lau, W., Jones, A. J., *Anal. Biochem.* 2009, *389*, 40–51.

[5] Chen, F. T., Evangelista, R. A., *Electrophoresis* 1998, *19*, 2639–2644.

[6] Guttman, A., *Electrophoresis* 1997, *18*, 1136–1141.

[7] Huang, Y., Mechref, Y., Novotny, M. V., *Anal. Chem.* 2001, *73*, 6063–6069.

[8] Yagi, Y., Yamamoto, S., Kakehi, K., Hayakawa, T., Ohyama, Y., Suzuki, S., *Electrophoresis* 2011, *32*, 2979–2985.

[9] Hase, S., Ikenaka, T., Matsushima, Y., *J. Biochem.* 1981, *90*, 407–414.

[10] Nakagawa, H., Kawamura, Y., Kato, K., Shimada, I., Arata, Y., Takahashi, N., *Anal. Biochem.* 1995, *226*, 130–138.

[11] Takahashi, N., Khoo, K. H., Suzuki, N., Johnson, J. R., Lee, Y. C., *J. Biol. Chem.* 2001, *276*, 23230–23239.

[12] Tomiya, N., Kurono, M., Ishihara, H., Tejima, S., Endo, S., Arata, Y., Takahashi, N., *Anal. Biochem.* 1987, *163*, 489–499.

[13] Yodoshi, M., Oyama, T., Masaki, K., Kakehi, K., Hayakawa, T., Suzuki, S., *Anal. Sci.* 2011, *27*, 395–400.

[14] Yodoshi, M., Tani, A., Ohta, Y., Suzuki, S., *J. Chromatogr. A* 2008, *1203*, 137–145.

[15] Honda, S., Suzuki, S., *Anal. Biochem.* 1984, *142*, 167–174.

[16] Birrell, H., Charlwood, J., Lynch, I., North, S., Camilleri, P., *Anal. Chem.* 1999, *71*, 102–108.

[17] Wang, W. T., Ledonne, N. C., Ackerman, B., Sweeley, C. C., *Anal. Biochem.* 1984, *141*, 366–381.

[18] Suzuki, S., Honda, S., *Electrophoresis* 1998, *19*, 2539–2560.

[19] Hoffstetter-Kuhn, S., Paulus, A., Gassmann, E., Widmer, H. M., *Anal. Chem.* 1991, *63*, 1541–1547.

[20] Honda, S., Suzuki, S., Kakehi, K., *J. Chromatogr.* 1981, *226*, 341–350.

[21] Fournet, B., Montreuil, J., Strecker, G., Dorland, L., Haverkamp, J., Vliegenthart, J. F. G., Binette, P., Schmid, K., *Biochemistry* 1978, *17*, 5206–5214.

[22] Nakano, M., Kakehi, K., Tsai, M. H., Lee, Y. C., *Glycobiology* 2004, *14*, 431–441.

[23] Townsend, R. R., Hardy, M. R., Cumming, D. A., Carver, J. P., Bendiak, B., *Anal. Biochem.* 1989, *182*, 1–8.

[24] Spiro, R. G., Bhoyroo, V. D., *J. Biol. Chem.* 1974, *249*, 5704–5717.

[25] Green, E. D., Adelt, G., Baenziger, J. U., Wilson, S., Van Halbeek, H., *J. Biol. Chem.* 1988, *263*, 18253–18268.

[26] Tai, T., Yamashita, K., Ito, S., Kobata, A., *J. Biol. Chem.* 1977, *252*, 6687–6694.

[27] Tai, T., Yamashita, K., Ogata-Arakawa, M., Koide, N., Muramatsu, T., Iwashita, S., Inoue, Y., Kobata, A., *J. Biol. Chem.* 1975, *280*, 8569–8575.

[28] Yamashita, K., Tachibana, Y., Kobata, A., *J. Biol. Chem.* 1978, *253*, 3862–3869.

[29] Koller, A., Khandurina, J., Li, J., Kreps, J., Schieltz, D., Guttman, A., *Electrophoresis* 2004, *25*, 2003–2009.

[30] Honda, S., Akao, E., Suzuki, S., Okuda, M., Kakehi, K., Nakamura, J., *Anal. Biochem.* 1989, *180*, 351–357.

Journal of Chromatography A, 1309 (2013) 76–83

Contents lists available at ScienceDirect

Journal of Chromatography A

journal homepage: www.elsevier.com/locate/chroma

Quality assurance of monoclonal antibody pharmaceuticals based on their charge variants using microchip isoelectric focusing method

Mitsuhiro Kinoshita[a], Yuki Nakatsuji[a], Shigeo Suzuki[a], Takao Hayakawa[b], Kazuaki Kakehi[a,*]

[a] Faculty of Pharmacy, Kinki University, Kowakae 3-4-1, Higashi, Osaka 577-8502, Japan
[b] Pharmaceutical Research and Technology Institute, Kinki University, Kowakae 3-4-1, Higashi, Osaka 577-8502, Japan

ARTICLE INFO

Article history:
Received 13 June 2013
Received in revised form 25 July 2013
Accepted 6 August 2013
Available online 13 August 2013

Keywords:
Antibody
Isoelectric focusing
Microchip
Charge variant

ABSTRACT

Monoclonal antibody (mAb) pharmaceuticals are much more complex than small-molecule drugs. Such complex characteristics raise challenging questions for regulatory evaluation. Although heterogeneity in mAbs based on their charge variants has been mainly evaluated using gel-based isoelectric focusing (IEF) method, recent development in capillary electrophoresis and microchip electrophoresis has made it possible to assure their heterogeneities in more easy and rapid manner. In the present paper, we customized the imaged microchip isoelectric focusing (mIEF) for the analysis of mAbs, and compared the customized version with the conventional capillary isoelectric focusing (cIEF) method, and found that mIEF has much higher performance in operations, and its resolving powers are comparable with those obtained by cIEF.

1. Introduction

Clinical success of monoclonal antibody (mAb) pharmaceuticals has been transforming the pharmaceutical industries. In 2010, worldwide sales of all biologics including mAbs reached the US $100 billion mark [1].

mAb is a large glycoprotein molecule, and has complex tertiary structure due to various post-translational modifications [2]. In addition, during manufacturing processes and storage periods of an mAb product, it is well known that modifications such as deamidation, C-terminal lysine variants, N-terminal pyroglutamate, glycation, and glycosylation are observed individually and/or simultaneously [3,4]. These modifications lead changes of charge heterogeneity in mAbs, and result in changes of the product characteristics, like long-term stability and binding activity. Thus detailed monitoring and controlling these modifications which can affect mAbs' characteristics are mandatory requirement by regulatory agencies [5].

For evaluation of charge heterogeneities in glycoproteins, slab gel isoelectric focusing (IEF) developed by Svensson in early 1960s [6] has been a major technique, and still widely being employed in the development of protein-based biopharmaceutical products for lot release, stability testing, formulation screening, process development, comparability assessment, and product characterization. However, slab gel IEF method is time consuming and labor intensive. In addition, quantitative evaluation of the observed bands (spots) is not practical. Thus, most biopharmaceutical companies have shifted efforts into developing capillary based IEF assays. The capillary isoelectric focusing (cIEF) method was first introduced in 1985 by Hjerten and Zu using on-line direct UV detection [7]. The method involves a two-step process: the analytes are first focused in the capillary, and then the focused proteins are forced to move toward the on-line UV detector. This cIEF method is more robust, reproducible, and quantitative than slab gel IEF, and it has been successfully applied to many therapeutic glycoproteins including mAbs [5,8–10].

A different cIEF technique called imaged cIEF which employs the whole capillary imaging technology to detect the focused protein without the mobilization step was first demonstrated by Wu and Pawliszyn in 1992 [11,12]. The imaged capillary isoelectric focusing (icIEF) method is faster than the conventional on-line detection cIEF (typically, total run time is 20 min versus 60 min, respectively). Reproducibilities in the icIEF method are slightly better than cIEF, because icIEF method does not require mobilization step that causes disruption of pH gradient and diffusion of focused samples. The icIEF technology has been increasingly used in the field of biopharmaceuticals, and it is now becoming one of the tools to evaluate charge heterogeneity for the evaluation of many therapeutic glycoprotein products [13–15] and protein-based vaccines [16,17].

* Corresponding author. Tel.: +81 6 4307 4001; fax: +81 6 6721 2353.
E-mail address: k_kakehi@phar.kindai.ac.jp (K. Kakehi).

0021-9673/$ – see front matter © 2013 Elsevier B.V. All rights reserved.
http://dx.doi.org/10.1016/j.chroma.2013.08.021

A quartz microchip-based apparatus with a linear imaging UV photodiode array detection (Shimadzu MCE-2010 system) was also commercially available and used in the IEF analysis of proteins. Vlcková et al. reported the results of IEF analysis of some biopharmaceuticals using the installed quartz microchip coated with linear polyacrylamide [18]. Three therapeutic proteins, hirudin, erythropoietin, and bevacizumab as a model of mAb were successfully analyzed, and the results were compared with conventional capillary IEF in terms of peak profile, isoelectric point (p*I*) values, and reproducibility. Kitagawa et al. reported high-speed analysis of some proteins by a customized microchip IEF apparatus [19], which has a devise for a simple straight channel chip. A standard mixture of some proteins was successfully separated into individual proteins having different p*I* values.

Based on these previous works, we customized the microchip apparatus for routine works in evaluation of charge variants of mAb products. And an ultra-fast charge variant profiling which enables to evaluate biopharmaceutical glycoprotein products was estimated. The quartz chip having simple, short, and straight non-coated channel with whole column imaging detection system was investigated in terms of assay speed, throughput and the charge profiles, and the results were compared with those acquired by cIEF.

In addition, effects of the attached glycans and C-terminal lysine residues on charge varients of mAbs were also investigated. This is important information for evaluation of quality of mAb products.

2. Materials and methods

2.1. Reagents

All mAb products, bevacizumab, trastuzumab and cetuximab, were kindly donated by Kinki University Nara Hospital. Transferrin (human blood plasma) was purchased from Sigma–Aldrich (St. Louis, MO). Carrier ampholytes, ranges of pH 3–10, 5–8 and 8–10.5, were obtained from GE Healthcare (Buckinghamshire, UK). All p*I* markers (p*I* = 5.12, 7.40, 8.18, 9.22, and 10.10) were from ProteinSimple (Santa Clara, CA). Iminodiacetic acid and hydroxypropyl methyl cellulose (HPMC; viscosity of 2% aqueous solution at 20 °C, 4000 cP) were purchased from Tokyo Kasei (Chu-o-ku, Tokyo, Japan) and Sigma–Aldrich, respectively. All other reagents, L-arginine, L-aspartic acid, sodium hydroxide, phosphoric acid, *N,N,N′,N′*-tetramethylethylene-diamine (TEMED) were from Wako Pure Chemical Industries (Dosho-machi, Osaka, Japan). Peptide-N^4-(acetyl-β-D-glucosaminyl) asparagine amidase (PNGase F, EC 3.5.1.52, recombinant) and carboxypeptidase B (EC 3.4.17.2) were from Roche Diagnostics (Mannheim, Germany). Sialidase (from *Arthrobacter ureafacience*) was purchased from Nakalai Tesque (Nakagyo-ku, Kyoto, Japan).

2.2. mIEF instrument

On-chip measurements were performed on a commercial Shimadzu microchip electrophoresis system MCE-2010 (Kyoto, Japan), in which the chip design and the device for application of voltage are modified for charge profiling purpose. The D_2-lamp based instrument possesses a diode array detector with 1024 elements located along the separation channel, and it provides a linear imaging UV detection during electrophoresis [20]. A non-coated quartz microchip (Fig. 1a) having two 9 μL reservoirs at the each end of a simple, short, and straight separation channel, was provided from Shimadzu. The chip does not have the injection device, because the whole analytical path is filled with the sample solution. Changing the chip design as shown in Fig. 1 shows the best ability in isoelectric focusing (IEF) analysis. The semielliptical channel fabricated onto a quartz-chip plate is 25-μm depth and 60-μm width as shown in Fig. 1b. The effective separation length and the imaging detection window are 27 mm and 25.6 mm, respectively. There are two platinum electrodes on the chip to apply voltages between the anolyte and catholyte reservoirs.

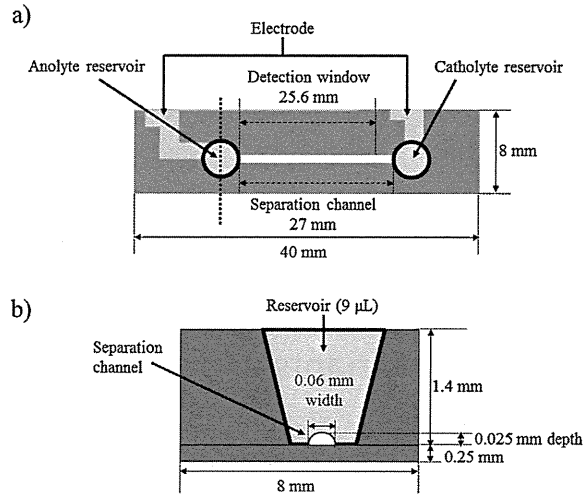

Fig. 1. (a) A quartz microchip specialized for isoelectric focusing, and (b) a scheme of a separation channel and a reservoir. Separated sample zones are monitored during electrophoresis within the detection window of 25.6 mm from the anolyte reservoir.

2.3. Preparation of the sample solution for IEF analyses

All mAb preparations were desalted by passing the solution through an ultrafiltration filter (Vivaspin 500; molecular weight cut-off: 100,000, GE Healthcare), and diluted with water to make aqueous 10 mg/mL solutions. The aqueous solution of transferrin (10 mg/mL) was also prepared in the same manner. The desalting procedure is especially important to obtain robust results in mIEF.

Sample solutions for mIEF analysis were prepared by mixing the protein solution with pharmalytes (pH 3–10, 5–8, and 8–10.5), HPMC solutions at different concentrations, suitable two p*I* markers (1 μL each) that are observed at both acidic and basic ends of the mAb peaks, 200 mmol/L arginine and water. For cIEF analysis, 4 μL of pharmalyte 3–10, 2 μL of TEMED, 200 μL of 0.8% (w/v) HPMC, 1 μL of two p*I* markers and 8 μL of 10 mg/mL antibody solution were mixed and diluted with water to make 400 μL of sample solutions. Final concentrations of each component are: 1% (v/v) pharmalyte 3–10, 0.5% (v/v) TEMED, 0.4% (w/v) HPMC, and 0.2 mg/mL mAb.

2.4. Digestion of cetuximab with carboxypeptidase B and sialidase

For hydrolysis of C-terminal lysine residue on heavy chain, a solution of cetuximab (10 mg/mL, 100 μL) was diluted with 20 mM phosphate buffer (pH 7.2, 100 μL), and mixed with 2 μL of carboxypeptidase B solution (1.5 U). The mixture was incubated at 37 °C for 12 h. After enzyme reaction, the reaction mixture was dialyzed against distilled water and lyophilized to dryness. The solution of carboxypeptidase-treated cetuximab (10 mg/mL, 100 μL) was diluted with 20 mM sodium acetate buffer (pH 5.0, 100 μL), and mixed with 2 μL of sialidase solution (2 mU). The mixture was kept at 37 °C for 12 h, and dialyzed against distilled water, and lyophilized to dryness. The dried samples thus obtained were

Table 1
Stepwise applied voltage for mIEF.

Peptide marker		Transferrin		mAbs	
Time (s)	Voltage (V)	Time (s)	Voltage (V)	Time (s)	Voltage (V)
0–20	130	0–20	130	0–20	100
20–100	250	20–40	250	20–120	200
100–240	500	40–100	500	120–220	390
		100–200	1000	220–270	780
				270–380	1560

dissolved in distilled water to make 10 mg/mL concentration, and used for the analysis.

2.5. mIEF analysis

A bare silica chip was employed throughout all mIEF experiments. Prior to the mIEF measurement, both channel and reservoirs were rinsed with water 3 times from one end of the channel by applying suitable pressure using a syringe filled with water. Between measurements, the chip was rinsed with water 5 times. After removing water by applying air pressure with a syringe, the anolyte reservoir was filled with the sample solution and pressure was applied to the reservoir by a syringe in order to fill the channel with the sample solution. The anolyte and catholyte reservoirs were then emptied. And the anolyte reservoir was filled with anolyte (40 mmol/L of aspartic acid containing 1.0% (w/v) HPMC), and the catholyte reservoir was filled with catholyte (100 mmol/L of sodium hydroxide with 1.0% (w/v) HPMC). Focusing was performed by applying voltage as indicated in Table 1.

Microchip used in this study is specially modified and has a large reservoir volume (9 μL) for catholyte and anolyte. Therefore, applying of constant high electric field strength (e.g. 450 V/cm) causes current burst at early stage of electrophoresis. Adopted stepwise voltage program could reduce initial current burst which causes migration of sample ions toward cathode with electroosmotic flow, and also could keep constant current during focusing. Detection was performed at 280 nm with monitoring the progress of the separation. The final image of the IEF trace was then converted to a data file for data analysis.

2.6. cIEF analysis

A P/ACE capillary electrophoresis system (Beckman Coulter, Fullerton, CA) equipped with a filter-based UV detector set at 280 nm was applied for cIEF measurements. Separations were carried out at 20 °C using a commercially available DB-1 capillary (internal diameter, 50 μm, Agilent Technologies, Palo Alto, CA) with an effective length of 30 cm (total length, 40 cm). The capillary was rinsed with 6 mol/L urea for 10 min and then with water for 10 min prior to use. At the initial step, the capillary was filled with the sample solution by applying pressure (30 psi) for 2 min. During cIEF separation, 200 mmol/L of phosphoric acid containing 0.4% (w/v) HPMC was used as the anode buffer, and 300 mmol/L of sodium hydroxide containing 0.4% (w/v) HPMC was used as the cathode buffer. For focusing step, voltage at 25 kV in normal polarity was applied for 10 min to focus charge variants into their p*I* positions. For mobilization of the separated zones toward detection window, voltage at 25 kV in normal polarity was applied, and pressure at 0.5 psi was also added to both negative and positive ends of the capillary. The mobilized sample zones were detected at 280 nm. Between IEF analyses, the capillary was rinsed for 5 min with 6 mol/L urea, and then with water for 5 min. All the data were analyzed by 32 Karat software, version 8.0 (Beckman Coulter).

3. Results and discussion

3.1. Optimization studies for mIEF

At the initial step of optimization studies on mIEF analysis, transferrin (human, isoelectric point of the major isoform, ca. 5.4 [21]) was employed as model protein, because isoforms of transferrin have been extensively examined for clinical tests of chronic alcoholism [22–24]. Transferrin has two possible *N*-glycan attaching sites, and major *N*-glycans observed in transferrin are disialo-biantennary glycans, and trisialo-triantennary glycans are also present as minor glycans [25]. Four parameters (a) neutral polymer, (b) Pharmalyte, (c) mixing ratios of different p*I* range Pharmalyte, and (d) urea, were optimized (Table 2).

3.1.1. Effect of neutral polymer concentration

Hydroxypropylmethylcellulose (HPMC, a commonly used neutral polymer) was used as an additive for mIEF to reduce electroosmotic flow during separation. Addition of a neutral polymer in the running buffer covers the silica surface and prevents the irreversible adsorption of the protein molecules to the quartz channel [26–28]. Therefore, the presence of the neutral polymer in the electrolyte improves the sensitivity as well as durability of the quartz chip. The sample solution for mIEF was prepared by mixing an aqueous solution (10 mg/mL: 20 μL) of transferrin, 1 μL of p*I* markers (p*I* 5.12 and 7.40), and HPMC solutions containing different concentrations of Pharmalyte 5–8. Isoforms of transferrin were not resolved well in a range of 0–0.1% of HPMC probably due to non-specific adsorption of the protein to the channel wall (Fig. 2a-1 and -2), because the peak intensities are smaller than those observed at higher concentrations of HPMC. When higher concentrations than 0.4% of HPMC were used (Fig. 2a-4 and -5), peaks became broader probably due to molecular sieving effect provided by HPMC [29,30]. Yasui et al. investigated the correlation between electrophoretic mobility of non-denatured proteins and HPMC concentration below 1.0% [31], which is much lower than the reported entanglement point [32]. HPMC has amphiphilic properties, and shows non-specific interactions with proteins at high concentrations [31] (Fig. 2a-4 and -5). From these reasons, 0.2% HPMC concentration (Fig. 2a-3) was selected.

3.1.2. Pharmalyte concentration and its mixing ratios

In the present study, we chose Pharmalyte as carrier ampholyte due to the robustness in IEF analysis [5]. In order to achieve the best resolution among isoform peaks of transferrin, Pharmalyte concentration was investigated. At the lower concentrations than 1.0% of Pharmalyte, transferrin showed broad peak due to incomplete formation of pH gradient in the channel (Fig. 2b-1 and -2). On the other hand, broad peaks were also observed at the concentrations of 4.0% or 8.0% of Pharmalyte, although relatively sharp peaks of p*I* markers were observed (Fig. 2b-4 and -5). At 2.4% concentration of Pharmalyte, transferrin showed the similar electropherogram as reported previously [33] (Fig. 2b-3).

Table 2
Parameters on optimization studies in mIEF.

Parameter group	No.	HPMC concentration	Pharmalyte concentration	Mixing ratios of pharmalyte		Urea concentration (mol/L)
				5–8	3–10	
(a)	–1	0.0%	2.4%	1	0	0
	–2	0.1%	2.4%	1	0	0
	–3	0.2%	2.4%	1	0	0
	–4	0.4%	2.4%	1	0	0
	–5	0.8%	2.4%	1	0	0
(b)	–1	0.2%	0.5%	1	0	0
	–2	0.2%	1.0%	1	0	0
	–3	0.2%	2.4%	1	0	0
	–4	0.2%	4.0%	1	0	0
	–5	0.2%	8.0%	1	0	0
(c)	–1	0.2%	2.4%	1	0	0
	–2	0.2%	2.4%	4	1	0
	–3	0.2%	2.4%	9	1	0
	–4	0.2%	2.4%	19	1	0
(d)	–1	0.2%	2.4%	19	1	0
	–2	0.2%	2.4%	19	1	1
	–3	0.2%	2.4%	19	1	2

Mixing ratio of Pharmalyte products having different range of p*I*s to form the best pH gradient in the separation channel, is one of the key parameters to achieve the best resolution. Since transferrin possesses charge variants in a range of p*I* 5–7, several mixing ratios of Pharmalyte 3–10 and Pharmalyte 5–8 were examined. When Pharmalyte 3–10 and Pharmalyte 5–8 were used in 1:19 ratios (Fig. 2c-4), the best resolution of the peaks was observed as compared to the case using only Pharmalyte 5–8 (see Fig. 2b-3).

3.1.3. Addition of urea and TEMED

Urea is a commonly used additive for both cIEF and icIEF to increase solubility of hydrophobic proteins around their p*I* values [9,34], but urea denatures proteins, and often causes shifts of their p*I* values [11,35]. When urea was added to the separation mixture at 1 mol/L and 2 mol/L, p*I* values of the main peak were slightly shifted to the cathode and peak intensities were gradually decreased (Fig. 2d-2 and -3) probably due to denaturing of

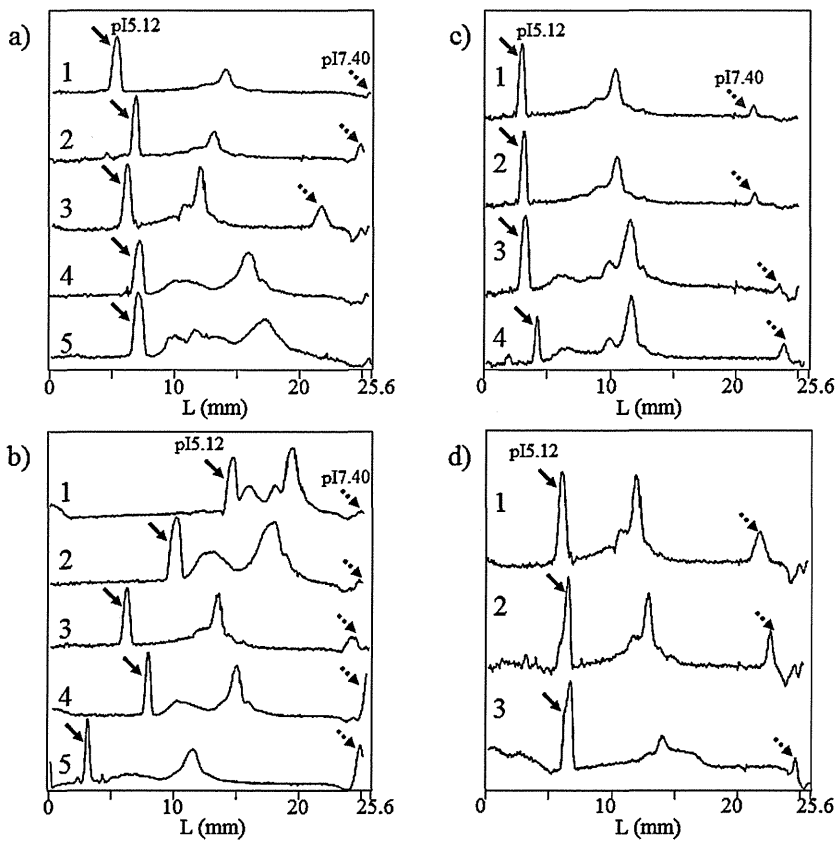

Fig. 2. mIEF separations at (a) several HPMC concentrations, (b) Pharmalyte concentrations, (c) Pharmalyte mixing ratios, and (d) urea concentrations in the separation mixture. Solid arrows and dashed arrows show p*I* markers of 5.12 and 7.40, respectively. (a) Sample solutions containing (1) 0%, (2) 0.1%, (3) 0.2%, (4) 0.4%, and (5) 0.8% HPMC as final concentration. (b) Sample solution containing (1) 0.5%, (2) 1.0%, (3) 2.4%, (4) 4.0%, and (5) 8.0% Pharmalyte as final concentration. (c) Sample solution containing Pharmalyte 3–10 and 5–8 at (1) 0:1, (2) 1:4, (3) 1:9, and (4) 1:19 ratios to make 2.4% Pharmalyte as final concentration. (d) Sample solution containing (1) 0 mol/L, (2) 1 mol/L, and (3) 2 mol/L urea as final concentrations. Analytical conditions: anolyte, 0.04 mol/L aspartic acid with 1% HPMC; catholyte, 0.1 mol/L sodium hydroxide with 1% HPMC; stepwise separation voltages were applied as shown in Table 1. Detection: UV absorption at 280 nm. Four parameters on optimization studies for mIEF are listed in Table 2.

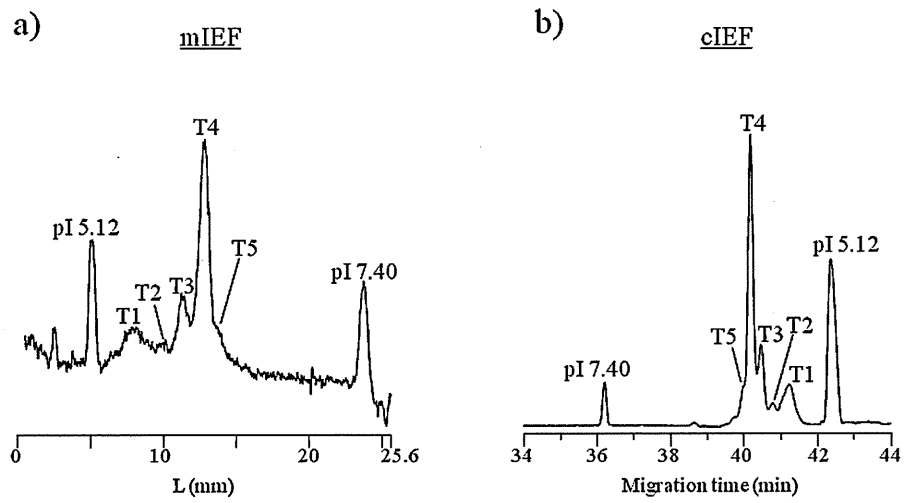

Fig. 3. mIEF (a) and cIEF (b) for profiling of charge variants of transferrin under optimized conditions. Peaks were labeled as T1 through T5 depending on their detection positions in mIEF. Smaller peak number means more acidic peak in the test sample. Analytical conditions for mIEF are the same as those in Fig. 2. Analytical conditions for cIEF: capillary, DB-1 capillary (Agilent Technologies), 50 μm I.D. with an effective length of 30 cm (total length, 40 cm); anolyte, 0.2 mol/L phosphoric acid with 0.4% HPMC; catholyte, 0.3 mol/L sodium hydroxide with 0.4% HPMC; injection, 2 min at 30 psi; focusing, 25 kV in normal polarity for 10 min; mobilization, 25 kV in normal polarity with pressure at 0.5 psi on both negative and positive ends of capillary; temperature, 20 °C; detection, UV at 280 nm.

transferrin in the presence of urea at high concentrations [36]. In the analysis of transferrin, urea is not necessary (Fig. 2d-1).

TEMED is often used as an additive for preventing focusing of basic proteins beyond the detection window in cIEFs and works as a spacer between the catholyte and the basic end of pH gradient [35,37]. However, addition of TEMED in the separation mixture at 0.4% concentration obviously decreased resolution (data not shown). Thus, TEMED is not necessary in the analysis of isoforms of transferrin in mIEF. However, in case of the analysis of basic proteins having higher p*I* values (p*I* > 10), TEMED is required as a spacer.

Based on the optimization studies on the analysis of transferrin, the sample solution was prepared as follows: 2.4% of Pharmalyte (5–8:3–10, 19:1), 0.2% of HPMC and 2 mg/mL of transferrin.

3.1.4. Analysis of isoforms of transferrin by mIEF and cIEF

Under the optimized conditions, transferrin was resolved into 5 isoforms within 200 s in a range of 5–15 mm from the anolyte reservoir (Fig. 3a). p*I* Values of the peaks were calculated by linear regression between p*I* 5.12 and 7.40 markers. Calculated p*I* value of the most abundant isoform (T4) was 6.06, and other isoforms (T1, T2, T3, and T5) were observed between p*I* 5.46 and 6.19 in mIEF analysis.

The calculated p*I* values obtained by mIEF were compared with those acquired by cIEF as shown in Fig. 3b. The difference (Δp*I*) of calculated p*I* values of the most abundant isoform (T4) was +0.14 (Table 3). And those of other isoforms (T1, T2, T3 and T5) ranged from −0.08 to +0.19. Thus, calculated p*I* values obtained by mIEF were comparable to those obtained by cIEF.

Sensitivities of the proposed mIEF system were slightly lower than those of cIEF system (see Fig. 3). The limit of detection (LOD) for transferrin (isoform T4) in mIEF was estimated to be ca. 0.2 mg/mL (as final concentration) from a signal to noise ratio (S/N = 3). On the other hand, LOD in cIEF was 0.005 mg/mL. Because the total length of the channel is 25 mm in mIEF, the amount of the injected sample is much smaller than cIEF. This is the major reason why high sensitivity is not achieved in mIEF. However, the proposed mIEF with linear imaging UV detection system does not need sample mobilization toward detection window which often causes diffusion of focused charge variants and disruption of pH gradient. Furthermore, we can monitor the progress of separations in the real-time manner, therefore, readily find the optimal conditions (see the movie for the analysis of transferrin in electronic supplementary materials).

3.1.5. Effect of the presence of arginine in the sample solution

Most isoforms of mAB preparations show p*I* values between p*I* 7 and p*I* 10. Prior to the analysis of mAb, pH gradient formed during mIEF was examined using four p*I* markers (p*I*s 7.40, 8.18, 9.22, and 10.10) for accurate determination of p*I* values [5]. mIEF separation was performed using a mixture prepared by 2.4 μL of pharmalyte 8–10.5, 34 μL of 0.6% HPMC, 1 μL of each p*I* marker,

Table 3
Comparisons of calculated p*I* values in mIEF and cIEF.

Peak number	p*I* values in mIEF (Δp*I*)			
	Transferrin	Bevacizumab	Trastuzumab	Cetuximab
1 (acidic end)	5.46 (−0.08)	7.96 (+0.09)	8.45 (−0.07)	7.57 (−0.12)
2	5.70 (± 0.00)	8.10 (+0.07)	8.57 (−0.05)	7.71 (−0.16)
3	5.88 (+0.06)	8.29 (+0.05)	8.76 (+0.02)	7.90 (−0.14)
4	6.06 (+0.14)	8.41 (−0.01)	8.89 (+0.04)	8.09 (−0.15)
5	6.19 (+0.19)	–	8.98 (+0.03)	8.26 (−0.16)
6	–	–	–	8.43 (−0.18)
7	–	–	–	8.57 (−0.19)
8 (basic end)	–	–	–	8.68 (−0.25)

p*I* values obtained by mIEF are shown in the table. Numbers shown in round bracket are the actual p*I* difference (Δp*I*) compared with those obtained by conventional cIEF method. Peaks observed in each sample were labeled depending on their detection positions as shown in Figs. 3 and 5. Peak 1 means the most acidic-end peak in the sample, but they were not identical charge variants among the tested samples.

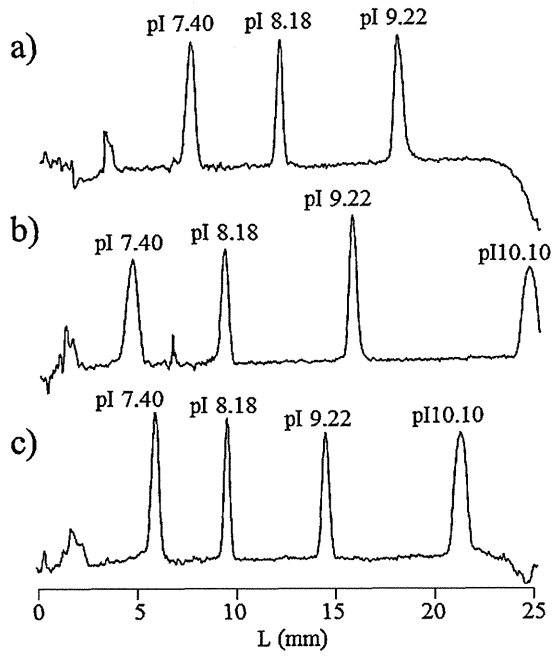

Fig. 4. mIEF separations of the mixture of four p*I* markers (p*I* 7.40, 8.18, 9.22, and 10.10) in the presence of (a) 0.0 mmol/L, (b) 4 mmol/L, and (c) 8 mmol/L arginine. Analytical conditions are the same as those in Fig. 2.

several volume of 200 mmol/L of arginine (p*I* = 10.76) which is commonly used as cathodic stabilizer [9] and water to make the sample solution to 100 μL. When analyzing the four p*I* markers without arginine, p*I* 10.10 marker was not detected due to leakage from the cathodic end (Fig. 4a). Addition of arginine to the mixture induced p*I* shift toward anodic end due to accumulated arginine zone at the cathodic end (Fig. 4b), and addition of 8 mmol/L of arginine showed the best separation of four p*I* markers within 240 s (Fig. 4c). Good linear relationship ($R^2 = 0.983$) was observed between the p*I* values and distances of the p*I* markers from the anolyte reservoir.

3.2. mIEF analysis of mAb pharmaceuticals

The optimized conditions employed for the analysis of transferrin was applied to the analysis of commercially available mAb products (bevacizumab, trastuzumab, and cetuximab). The analytical conditions were slightly modified based on the p*I* values of each mAB preparation.

For mIEF of mAb products, the mixture containing 2.4% pharmalyte 8–10.5, 0.2% HPMC, 8 mmol/L arginine and 2 mg/mL mAbs with two p*I* markers (p*I* 7.40 and 10.10) was employed as the sample solution. In bevacizumab, four charge variants (peak b1 to b4) were observed in both mIEF (Fig. 5a) and cIEF (Fig. 5b). p*I* values calculated by linear regression are summarized in Table 3. Δp*I* values were less than 0.09 for all observed peaks. And, relative abundances of the peaks (b1, b2, b3, and b4) were 4.0%, 23.5%, 69.2%, and 3.3% for mIEF, and were well correlated with the data observed by cIEF (5.0%, 24.9%, 64.8%, and 5.2%).

Other mAb products, trastuzumab (Fig. 5c) and cetuximab (Fig. 5e), were separated into five and eight charge variants by mIEF. Both electropherograms showed consistent profiles with those obtained by cIEF (Fig. 5d and f). The present data indicate that the proposed mIEF method is comparable to cIEF, and shows excellent ability in high-speed mAB analysis.

Table 4
Intra- and inter-day assay variations of mIEF.

	Calculated p*I* values			
	b1	b2	b3	b4
Repeatability (intra-day)				
1	7.86	8.03	8.25	8.45
2	7.83	8.00	8.22	8.42
3	7.86	8.03	8.22	8.44
Mean	7.85	8.02	8.23	8.44
RSD (%)	0.22	0.22	0.21	0.21
Reproducibility (inter-day)				
Day 1-1	7.86	8.02	8.22	8.43
Day 1-2	7.83	8.00	8.21	8.40
Day 1-3	7.86	8.04	8.22	8.43
Day 2-1	7.85	8.05	8.25	8.46
Day 2-2	7.86	8.05	8.23	8.46
Day 2-3	7.84	8.02	8.25	8.44
Day 3-1	7.86	8.03	8.25	8.45
Day 3-2	7.83	8.00	8.22	8.42
Day 3-3	7.86	8.03	8.22	8.45
Mean	7.85	8.03	8.23	8.44
RSD (%)	0.17	0.23	0.19	0.24

Peaks observed in bevacizumab were labeled as b1 through b4 depending on their detection positions as shown in Fig. 5a.

3.3. Precision of mIEF method

In order to evaluate the precision of the optimized mIEF method, repeatability and reproducibility were investigated using bevacizumab as a model mAb product. For repeatability assessment, a single separation mixture was prepared and analyzed using two p*I* markers of 7.40 and 9.22 instead of 10.10. On the other hand, for reproducibility assessment, separation mixtures were prepared in triplicate on each day, and analyzed by mIEF over three days as summarized in Table 4.

All four charge variants were separated each other within 380 s, and RSDs of the measured position (*L*, mm) ranged from 0.81% to 1.28% under optimized conditions (data not shown). After correction using p*I* markers, RSDs of calculated p*I* values were less than 0.25%. These values were comparable with those obtained by icIEF (0.2% or less in [15,38]). These data indicate that the proposed mIEF method shows excellent reproducibility, because the method does not require mobilization, and superior to those obtained by the conventional two-step cIEF [5]. In addition, RSDs of relative abundances of each peak (b1 to b4) in repeatability experiments (intra-day, $n = 3$) were 9.5%, 0.7%, 1.7%, and 11.5%, and in reproducibility executions (inter-day, $n = 9$) were 14.0%, 8.8%, 3.8%, and 16.6%, respectively. These values were similar to those reported previously using icIEF as described above.

3.4. Assessment of heterogeneity by sequential enzymatic digestions of mAb pharmaceuticals

C-Terminal lysine variants [39] and the presence of sialo *N*-glycans in mAb products [40] are the major reasons for charge variants. Two enzymes, carboxypeptidase B and sialidase, were used to understand charge heterogeneity of cetuximab. Digestion of cetuximab with carboxypeptidase B caused disappearance of two peaks (c7 and c8) at basic region (Fig. 6b).

In contrast, trastuzumab and bevacizumab (humanized antibody products manufactured by CHO cells) showed no significant changes (data not shown). These results are consistent with the previous report that relative amounts of incorporated C-terminal lysine in mAbs manufactured by CHO cell lines were up to 5% [40]. In addition, further digestion with sialidase resulted in

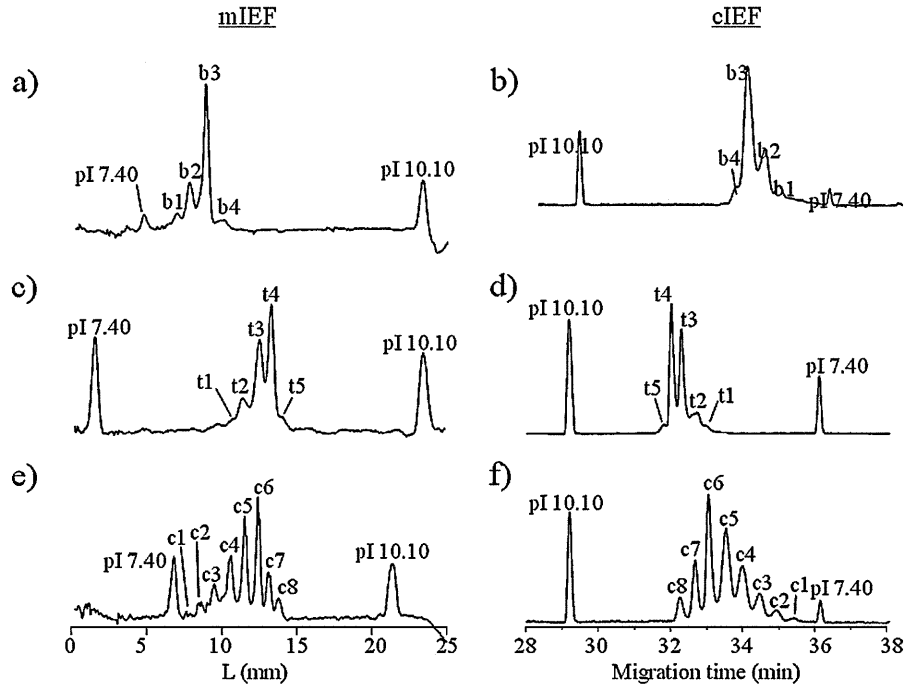

Fig. 5. Analysis of charge variants of bevacizumab, trastuzumab, and cetuximab by mIEF (left column) and cIEF (right column). Peaks observed in each sample were labeled with numbers depending on their detection positions. Peak 1 means the most acidic-end peak in the sample, but they were not identical charge variants among the tested samples. Analytical conditions are the same as shown in Fig. 2. Bevacizumab (a and b), trastuzumab (c and d) and cetuximab (e and f).

decrease/disappearance of the peaks observed in acidic p*I* regions (Fig. 6c). After successive digestion with these two enzymes, cetuximab gave the simple profile which is similar to that of bevacizumab and trastuzumab as shown in Fig. 5a and c. Thus, charge heterogeneity of cetuximab is largely due to C-terminal lysine processing and sialylation of *N*-glycans. These charge heterogeneities of cetuximab may be due to manufacturing process. Bevacizumab and trastumab are humanized mAb products (IgG_1), and produced by CHO cells. In contrast, cetuximab is chimeric mouse-human IgG_1 produced by mouse myeloma SP2/0 cell line. This means that manufacturing process change in cell type may lead significant alteration in mAb heterogeneity especially in charge variants. Several charge variants are still present in enzyme-treated cetuximab. Although cetuximab may include other possible modifications such as N-terminal glutamine cyclization, asparagine deamination, and methionine oxidation, detailed structural analysis will be necessary to get better understanding in heterogeneity of mAbs by analyzing fractionated peaks such as accurate mass spectrometric methods.

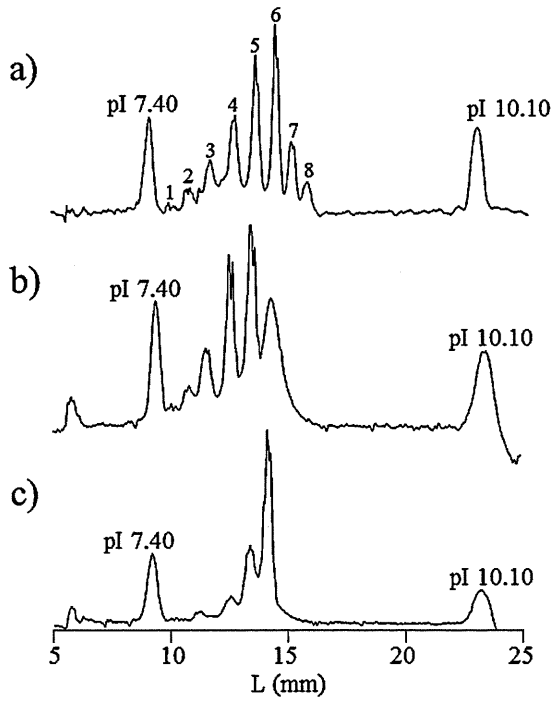

Fig. 6. mIEF separation of (a) intact, (b) carboxypeptidase B-treated, and (c) sialidase-treated cetuximab. Analytical conditions are the same as shown in Fig. 2.

4. Conclusion

A combination of a quartz chip specialized for isoelectric focusing and a microchip electrophoresis system with a whole column imaging UV photodiode array detector achieved ultrafast evaluation of charge variants of glycoproteins. The quartz chip having a simple, short and straight channel without any coating could resolve transferrin and three mAb pharmaceuticals into their charge variants within 200 s and 380 s with high reproducibility in terms of calculated p*I* values and percent relative amounts of each charge variant.

Charge profiles of protein samples determined by mIEF well corresponded to those obtained by cIEF. When comparing precision in p*I* determination in mIEF measurements with icIEF measurements (e.g. commercially available iCE280 Analyzer), and cIEF, reproducibility of the calculated p*I* values is comparable to the iCE280 and superior to cIEF [15,38]. It should be noted that the time required for the analysis is much shorter than cIEF (approximately 10 times), which requires mobilization step after completion of focusing, and faster than icIEF (about 3 times) due to incorporation of shorter separation channel. Whole column imaging UV photodiode array detector leads precise tuning of focusing time, because the progress of the focusing can be monitored on the real-time basis. However, the proposed system needs to wash the chip manually, and further improvements in functionalization and

automation will be required for commercial use in the pharmaceutical industries. It is difficult to introduce enough amount of the sample due to short analytical channel. Improvement of the sensitivity is another future requirement.

Evaluation of charge heterogeneity is necessary for assurance of quality and stability of mAb products. Some charge variants derived from several post-translational modifications or degradation show different biological activity and stability compared to their original variants [41,42]. Isoelectric focusing based techniques such as mIEF, icIEF and cIEF makes us easy to access to useful information on product specific "fingerprint" derived from charge heterogeneity of biopharmaceuticals. To get much better understanding in detail into the therapeutics, further investigation such as structural analyses, potency, toxicity and stability evaluation will be required. Mass spectrometry is one of the powerful tools to satisfy these demands from the pharmaceutical industry, and fractionated/separated peaks need to be analyzed for further evaluation of their characterization.

The proposed ultrafast and precise mIEF method is easily applied to identity and purity analyses in product lot release, stability testing, formulation screening, process development, comparability assessment and product characterization of biopharmaceutical products possessing complex charge heterogeneity.

Acknowledgements

The authors would like to thank Dr. Eiki Maeda at Analytical Development Laboratories, CMC Center, Takeda Pharmaceutical Company Limited for experimental supports. The authors are also grateful to Shin Nakamura and Akihiro Arai at Life Science Business Department, Analytical & Measuring Instruments Division, Shimadzu Cooperation for providing microchip and measuring equipment.

Appendix A. Supplementary data

Supplementary data associated with this article can be found, in the online version, at http://dx.doi.org/10.1016/j.chroma.2013.08.021.

References

[1] S.A. Berkowitz, J.R. Engen, J.R. Mazzeo, G.B. Jones, Nat. Rev. Drug Discov. 11 (2012) 527.
[2] M. Mann, O.N. Jensen, Nat. Biotechnol. 21 (2003) 255.
[3] O.N. Jensen, Curr. Opin. Chem. Biol. 8 (2004) 33.
[4] J. Seo, K.-J. Lee, J. Biochem. Mol. Biol. 37 (2004) 35.
[5] E. Maeda, K. Urakami, K. Shimura, M. Kinoshita, K. Kakehi, J. Chromatogr. A 1217 (2010) 7164.
[6] H. Svensson, Acta Chem. Scand. 15 (1961) 325.
[7] S. Hjertén, M.-d. Zhu, J. Chromatogr. 346 (1985) 265.
[8] Y. Kuroda, H. Yukinaga, M. Kitano, T. Noguchi, M. Nemati, A. Shibukawa, T. Nakagawa, K. Matsuzaki, J. Pharm. Biomed. Anal. 37 (2005) 423.
[9] J. Lin, Q. Tan, S. Wang, J. Sep. Sci. 34 (2011) 1696.
[10] K.G. Moorhouse, C.A. Rickel, A.B. Chen, Electrophoresis 17 (1996) 423.
[11] J. Wu, J. Pawliszyn, Anal. Chem. 64 (1992) 2934.
[12] J. Wu, J. Pawliszyn, Anal. Chem. 64 (1992) 224.
[13] P. Dou, Z. Liu, J. He, J.-J. Xu, H.-Y. Chen, J. Chromatogr. A 1190 (2008) 372.
[14] X.Z. He, A.H. Que, J.J. Mo, Electrophoresis 30 (2009) 714.
[15] Z. Sosic, D. Houde, A. Blum, T. Carlage, Y. Lyubarskaya, Electrophoresis 29 (2008) 4368.
[16] L. Goodridge, C. Goodridge, J. Wu, M. Griffiths, J. Pawliszyn, Anal. Chem. 76 (2004) 48.
[17] Z. Liu, J. Pawliszyn, Electrophoresis 26 (2005) 556.
[18] M. Vlcková, F. Kalman, M.A. Schwarz, J. Chromatogr. A 1181 (2008) 145.
[19] F. Kitagawa, S. Aizawa, K. Otsuka, Anal. Sci. 25 (2009) 979.
[20] H. Nakanishi, T. Nishimoto, A. Arai, H. Abe, M. Kanai, Y. Fujiyama, T. Yoshida, Electrophoresis 22 (2001) 230.
[21] H. Stibler, Clin. Chem. 37 (1991) 2029.
[22] F. Crivellente, G. Fracasso, R. Valentini, G. Manetto, A.P. Riviera, F. Tagliaro, J. Chromatogr. B: Biomed. Sci. Appl. 739 (2000) 81.
[23] F. Tagliaro, F. Bortolotti, M. Zuliani, F. Crivellente, G. Manett, V.L. Pascali, M. Marigo, J. Capill. Electrophor. Microchip Technol. 6 (1999) 137.
[24] F. Tagliaro, F. Crivellente, G. Manetto, I. Puppi, Z. Deyl, M. Marigo, Electrophoresis 19 (1998) 3033.
[25] E. Landberg, E. Aström, B. Kågedal, P. Påhlsson, Clin. Chim. Acta: Int. J. Clin. Chem. 414C (2012) 58.
[26] S.R. Bean, G.L. Lookhart, Electrophoresis 19 (1998) 3190.
[27] P.G. Righetti, C. Gelfi, B. Verzola, L. Castelletti, Electrophoresis 22 (2001) 603.
[28] M. Viefhues, S. Manchanda, T.-C. Chao, D. Anselmetti, J. Regtmeier, A. Ros, Anal. Bioanal. Chem. 401 (2011) 2113.
[29] B. Deng, N. Ye, G. Luo, Y. Wang, J. Nanosci. Nanotechnol. 5 (2005) 1193.
[30] M.-Y. Ye, X.-F. Yin, Z.-L. Fang, Anal. Bioanal. Chem. 381 (2005) 820.
[31] T. Yasui, M. Reza Mohamadi, N. Kaji, Y. Okamoto, M. Tokeshi, Y. Baba, Biomicrofluidics 5 (2011) 441141.
[32] A.E. Barron, D.S. Soane, H.W. Blanch, J. Chromatogr. A 652 (1993) 3.
[33] E. Quintana, R. Montero, M. Casado, A. Navarro-Sastre, M.A. Vilaseca, P. Briones, R. Artuch, J. Chromatogr. B: Anal. Technol. Biomed. Life Sci. 877 (2009) 2513.
[34] S. Mack, I. Cruzado-Park, J. Chapman, C. Ratnayake, G. Vigh, Electrophoresis 30 (2009) 4049.
[35] A. Cifuentes, M.V. Moreno-Arribas, M. de Frutos, J.C. Díez-Masa, J. Chromatogr. A 830 (1999) 453.
[36] A. Pantazaki, M. Taverna, C. Vidal-Madjar, Anal. Chim. Acta 383 (1999) 137.
[37] A. Bossi, P.G. Righetti, C. Visco, U. Breme, M. Mauriello, B. Valsasina, G. Orsini, E. Wenisch, Electrophoresis 17 (1996) 932.
[38] N. Li, K. Kessler, L. Bass, D. Zeng, J. Pharm. Biomed. Anal. 43 (2007) 963.
[39] L.W. Dick, D. Qiu, D. Mahon, M. Adamo, K.-C. Cheng, Biotechnol. Bioeng. 100 (2008) 1132.
[40] E. Maeda, S. Kita, M. Kinoshita, K. Urakami, T. Hayakawa, K. Kakehi, Anal. Chem. 84 (2012) 2373.
[41] G. Janini, N. Saptharishi, M. Waselus, G. Soman, Electrophoresis 23 (2002) 1605.
[42] P.A. Trail, H.D. King, G.M. Dubowchik, Cancer Immunol. Immunother. 52 (2003) 328.

Journal of Chromatography B, 928 (2013) 16–21

Contents lists available at SciVerse ScienceDirect

Journal of Chromatography B

journal homepage: www.elsevier.com/locate/chromb

Free glycans derived from glycoproteins present in human sera

Kinya Iwatsuka[a], Sakie Watanabe[a], Mitsuhiro Kinoshita[a], Kazuya Kamisue[a], Keita Yamada[a], Takao Hayakawa[b], Tadashi Suzuki[c], Kazuaki Kakehi[a,*]

[a] Faculty of Pharmaceutical Sciences, Kinki University, 3-4-1 Kowakae, Higashi-Osaka 577-8502, Japan
[b] Pharmaceutical Research and Technology Institute, Kinki University, Kowakae 3-4-1, Higashi-osaka 577-8502, Japan
[c] Glycometabolome Laboratory, Frontier Research System, RIKEN (The Institute for Physical and Chemical Research), 2-1 Hirosawa, Wako, Saitama 351-0198, Japan

ARTICLE INFO

Article history:
Received 15 December 2012
Accepted 12 March 2013
Available online 21 March 2013

Keywords:
Free glycans
Serum
Transferrin
HPLC
ESI-TOF-MS

ABSTRACT

During the course of studies on the analysis of O-glycans in biological samples, we found that significant amount of free glycans are present in normal human serum samples. The most abundant free glycan was disialo-biantennary glycan typically observed in transferrin which is one of the abundant glycoproteins found in sera. Minor glycans were also considered to be mainly due to transferrin, but some glycans were derived from mucin-type O-glycans, although the amount was quite minute. However, high mannose-type glycans could not be detected at all. Although there have been many reports on the presence of intracellular "free" N-glycans (mainly derived from high mannose-type glycans) generated either from lipid-linked oligosaccharides or from misfolded glycoproteins through endoplasmic-reticulum associated protein degradation pathway, there is little information on the presence of free glycans in extracellular matrix and biological fluids such as serum. This report is the first one which demonstrates the presence of free glycans due to glycoproteins in sera.

1. Introduction

There have been many reports on the presence of free glycans in cytosols, and the formation of such free glycans is an important clue for the understanding the selection of properly synthesized glycoproteins. Such free glycans found in cytosols are exclusively high mannose-type glycans having one N-acetylglucosamine (GlcNAc) residue at the reducing termini [1,2], and are formed in the cytosol by a cellular system called ERAD (endoplasmic reticulum-associated degradation) [3]. Such intracellular "free" N-glycans are generated either from lipid-linked oligosaccharides or from misfolded glycoproteins [4–7]. In both cases, occurrence of high mannose-type free glycans, which have one GlcNAc residue at their reducing ends, has been well-documented.

Little is known with regard to the accumulation of more processed, complex-type free glycans in the cytosol of mammalian cells. In our previous report on the comprehensive analysis of N-glycans in cancer cells [8], we found that significantly large amount of unusual, complex-type free N-glycans were accumulated in stomach cancer-derived cell lines, MKN7 and MKN45. It should be noticed that all the free glycans found in these cells were cleaved between the GlcNAcβ1–4GlcNAc (i.e. chitobiose) bond and a single GlcNAc residue was present at the reducing end. In addition, most of the accumulated glycans have N-acetylneuraminic acid (NeuAc) residues at the non-reducing termini. And we showed that loss of the activity of cytosolic neuraminidase, Neu2, was responsible for the accumulation of such unusual free glycans [9].

In contrast, there is little information on the presence of free glycans in extracellular matrixes and biological fluids such as sera probably due to insufficient and poor ability to analyze minute amount of glycans. We have been developing sensitive methods for comprehensive analyses of N- and O-glycans in biological samples, especially cancer cells, tissues and serum samples [5,10–13]. During the course of studies on the analysis of O-glycans in biological samples, we found that significant amount of free glycans are present in human serum samples. This is unexpected and interesting, although it is well known that patients suffering from genetic lysosomal disorders of complex carbohydrate metabolism excrete a considerable amount of unusual oligosaccharides in urine [14–17].

Inoue et al. reported that free glycans were present in the unfertilized eggs of a fresh water trout, *Plecogiossus altivelis* [18]. The isolated glycans consist of desialylated biantennary glycans with β-Man-GlcNAc structure at their reducing termini. However, a small portion of the glycans having chitobiose (GlcNAcβ1-4-GlcNAc) structure at the reducing ends were also present. It is still not clear why and how such large amount of free glycans are accumulated in unfertilized eggs. Another important report on the presence of free glycans is the expression of free glycans in human seminal

* Corresponding author. Tel.: +80 6 6721 2332; fax: +80 6 6721 2353.
E-mail address: k_kakehi@phar.kindai.ac.jp (K. Kakehi).

1570-0232/$ – see front matter © 2013 Elsevier B.V. All rights reserved.
http://dx.doi.org/10.1016/j.jchromb.2013.03.010

plasma [19], and the structural characteristics are similar to those in human milk. But their variations are simpler than those of human milk oligosaccharides.

According to the reference search works on the presence of free glycans in sera, the present work demonstrating the presence of free glycans in sera is the first one, and will lead to a new research project on finding glycan-based disease biomarkers.

2. Materials and methods

2.1. Materials

Sephadex LH-20 and Asahi Shodex NH2P-50 4E column were obtained from GE Healthcare UK Ltd. (Buckinghamshire, UK) and Showa Denko (Minato-ku, Tokyo, Japan), respectively. Sodium cyanoborohydride and 2-aminobenzoic acid (2AA) were from Tokyo Kasei Kogyo (Chuo-Ku, Tokyo, Japan). TOYOPAK ODS-S for solid phase extraction was from Tosoh (Minato-ku, Tokyo, Japan). VIVASPIN 500 (3000 molecular weight cut off) for ultrafiltration was from Sigma–Aldrich Japan (Shinagawa-ku, Tokyo, Japan). All other reagents were of the highest grade commercially available. All aqueous solutions were prepared using water purified with a Milli-Q purification system (Millipore, Bedford, MA, USA).

2.2. Serum samples

Serum samples from healthy volunteers were obtained under the permission of the Ethics Committee of Kinki University School of Pharmacy, and used in accordance with the tenets of the Declaration of Helsinki.

2.3. Sample preparation

2.3.1. Ultrafiltration and solid-phase extraction of the serum sample

Because the serum sample contains a large amount of low-molecular-weight materials such as monosaccharides (typically glucose) and inorganic salts, and hydrophobic compounds, these materials should be removed prior to the analysis.

A serum sample (25 μL) was centrifuged at 15,000 × *g* using an ultramembrane filter (3000 molecular weight cut off) to remove the low-molecular weight materials, and concentrated to the one fourth volume. Water (150 μL) was added to the concentrate on the membrane, and centrifuged at 15,000 × *g* again. The procedures were repeated three times. The concentrated serum sample on the membrane was transferred to a new tube, and the membrane was washed with water (150 μL) and combined with the concentrated solution. The mixture was then passed through an ODS cartridge (90 mg) which was previously washed with methanol (0.8 mL 3×) and water (0.8 mL 3×). The clean-up procedures were performed according to the method recommended by the manufacturer.

2.3.2. Total N-glycans in a serum sample

A serum sample (150 μL) was centrifuged at 15,000 × *g* using an ultramembrane filter (3000 molecular weight cut off) to remove the low-molecular weight materials, and concentrated to dryness. The dried sample was suspended in water (200 μL) and was mixed with 10% SDS (24 μL) and 2-mercaptoethanol (2.4 μL). The mixture was kept in the boiling water bath for 5 min. After cooling, 10% NP40 (nonylphenol poly(ethylene glycol ether)$_n$) solution (24 μL) and 1 M sodium phosphate buffer (pH 7.5, 29 μL) were added. After addition of N-glycoamidase F (2 units), the mixture was kept at 37 °C overnight. After cooling, ethanol (695 μL) was added and the mixture was centrifuged at 15,000 × *g* for 10 min. The supernatant was collected and evaporated to dryness under reduced pressure.

2.3.3. Releasing reaction of O-glycans in mucin-type glycoproteins in serum samples

Releasing reaction of O-glycans from mucin-type glycoproteins present in serum samples was performed using the automated glycan releasing system according to the method reported previously [10].

2.3.4. Fluorescent labeling of glycans with 2AA

The sample of glycan mixture was dissolved in water (20 μL) and 2AA solution (100 μL) which was freshly prepared by dissolution of 2AA (15 mg) and sodium cyanoborohydride (15 mg) in methanol (500 μL) containing 4% sodium acetate and 2% boric acid. The mixture was kept at 80 °C for 1 h, and water (20 μL) and 50% (v/v) methanol (200 μL) were added to the mixture after cooling, and centrifuged at 15,000 × *g* for 10 min. The supernatant solution was applied to a column of Sephadex LH-20 (1.0 cm i.d., 30 cm length), which was previously equilibrated with 50% methanol. The earlier eluted fluorescent fractions were pooled and evaporated to dryness under reduced pressure. The residue was further purified by solid phase extraction as described above (Section 2.3.1), and evaporated to dryness.

2.3.5. Digestion of the glycan mixture with neuraminidase

Neuraminidase (1 munit, 2 μL) was added to the mixture of 2AA-labeled glycans in 20 mM acetate buffer (pH 5.0, 20 μL), and the mixture was incubated at 37 °C overnight. After keeping the mixture in the boiling water bath for 10 min followed by centrifugation, the supernatant solution was used for MS analysis.

2.4. HPLC analysis of 2AA-labeled free glycans and N-glycans in serum samples

Analysis of the 2AA-labeled glycans was performed with two Shimadzu LC-10ADvp pumps, a Jasco FP-920 fluorescence detector equipped with a polymer-based Asahi Shodex NH2P-50 4E column (4.6 mm i.d. × 250 mm). Linear gradient method was employed by 2% acetic acid in acetonitrile (solvent A) and 5% acetic acid in water containing 3% triethylamine (solvent B). The column was initially equilibrated and eluted with 30% solvent B for 2 min. Then, solvent B was increased to 95% over 80 min, and kept at this composition for further 20 min. The column effluent was monitored by a fluorescence detector set at an excitation wavelength of 350 nm and 425 nm for emission.

2.5. Liquid chromatography–electrospray ionization ion-trap time-of-flight mass spectrometry (LC–ESI-IT-TOF MS)

Negative electrospray ionization (ESI)-MS analyses were conducted with an LC–IT-TOF MS instrument (Shimadzu) connected with an HPLC system (LC-20AD pump and CBM-20A system controller; Shimadzu). The 2AA-labeled glycans were analyzed by infusion method. Isocratic elution was carried out at a flow rate of 0.2 mL/min with 50% (v/v) acetonitrile in water. The MS apparatus was operated at a probe voltage of 1.75 kV, CDL temperature of 180 °C, nebulizer gas flow of 1.5 L/min, ion accumulation time of 30 ms. MS range was from *m/z* 200 to 2000. CID parameters were as follows: energy, 50%; collision gas, 50%. MS data were processed with LCMS solution ver. 3.6 software (Shimadzu).

3. Results and discussion

3.1. Free glycans in serum samples

Fig. 1a shows the results on the analysis of O-glycans in a serum sample. In this analysis, O-glycans were previously

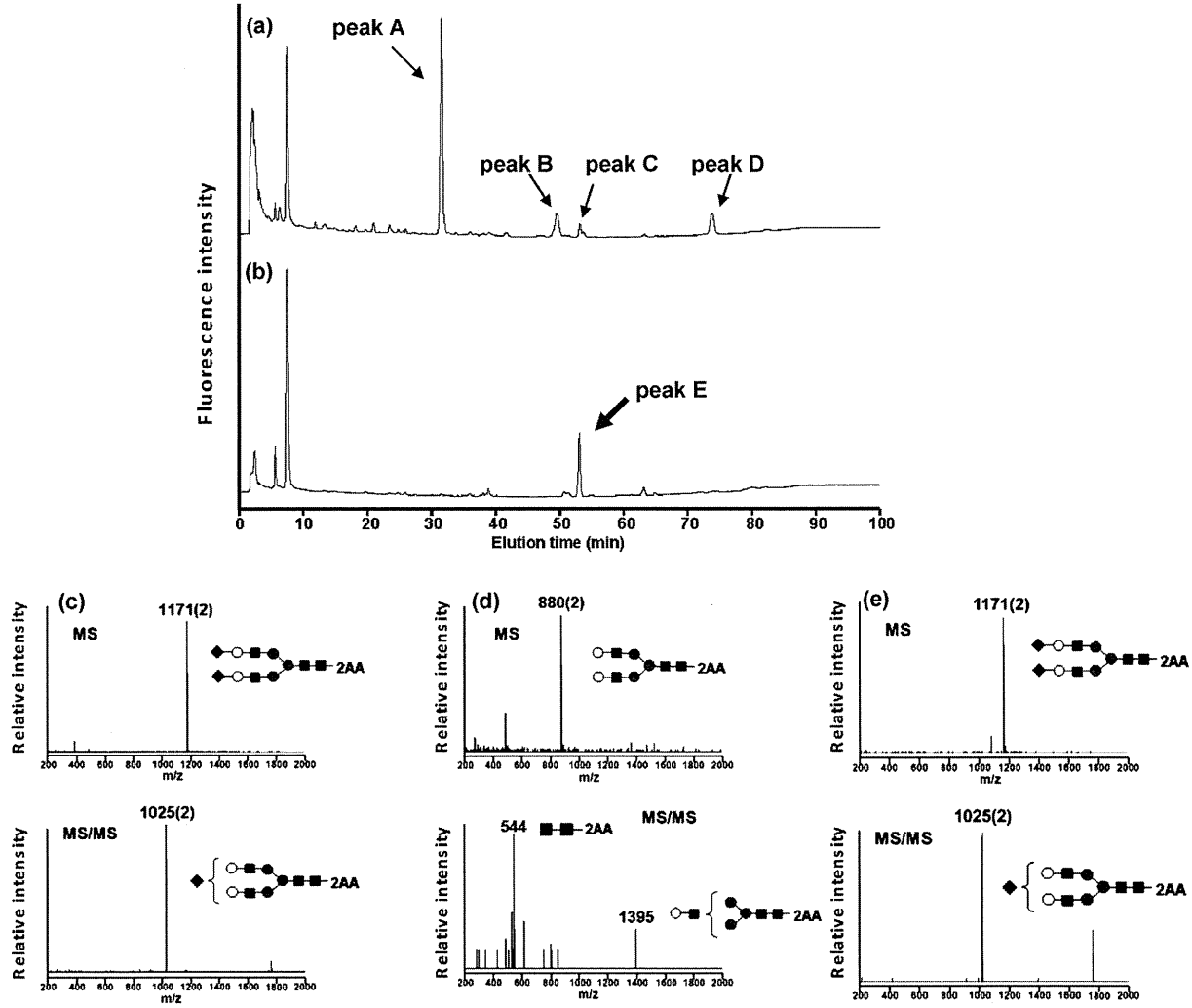

Fig. 1. HPLC Analysis of (a) mucin-type glycans from human serum released from the glycoproteins. (b) Intact serum sample after easy removal of low molecular weight materials. MS and MS/MS data of (c) peak C and (d) the product after neuraminidase digestion of peak C. (e) MS and MS/MS data of peak E. HPLC conditions: column, Asahi Shodex NH2P-50 4E(4.6 mm × 250 mm). Eluent solvent A, 2% acetic acid in acetonitrile, solvent B, 5% acetic acid, 3% triethylamine in water. Gradient condition: a linear gradient (30–95% solvent B) from 2 to 82 min, maintained for 20 min. Symbols: squares, N-acetylglucosamine; gray circles, mannose; white circles, galactose; diamonds, N-acetylneuraminic acid.

chemically released from the glycoproteins in a serum sample by an automatic manner developed by the authors [10–13], and analyzed by HPLC after labeling with a fluorescent reagent, 2AA. Four peaks (**A–D**) were detected at 30 (**A**), 46 (**B**), 53 (**C**) and 70 min (**D**), respectively. Peaks **A**, **B** and **D** were due to mucin-type O-glycans, and identified as sialyl T (NeuAcα2-3Galβ1-3GalNAc-2AA), degradation product (NeuAcα2–3 Gal) and disialyl T(NeuAcα2-3Galβ1-3[NeuACα2-6]GalNAc-2AA), respectively. A distinct peak (peak **C**) other than those of mucin-derived glycans was observed at 53 min. The MS and MS/MS spectra of the peak **C** are shown in Fig. 1c. The molecular ion of the peak was observed at *m/z* 1171 as a doubly charged ion, which was confirmed as disialo-biantennary glycan. And the ion due to monosialo biantennary glycan was observed in MS/MS spectra. The peak at 53 min was collected, and digested with neuraminidase. MS of the obtained asialoglycan showed the molecular ion at *m/z* 880 as a doubly charged ion (Fig. 1d). MS/MS spectra showed an ion due to chitobiosyl-2AA at *m/z* 544. These data clearly mean that peak **C** is due to disialobiantennary glycan. As indicated previously, the automatic apparatus employed for releasing O-glycans does not cleave Asn-GlcNAc linkage, and free N-glycans are not released from the protein core containing Asn-type glycoproteins [10]. This means that glycan (due to peak **C**) was endogenously present in serum samples.

To demonstrate if the glycans are due to free glycans in sera, the glycans in sera were directly analyzed after labeling with 2AA. After removing the small-molecular weight materials including glucose and inorganic salts in sera by ultrafiltration and also removing hydrophobic materials using an ODS-cartridge, the eluate (equivalent to 2 μL of sera) was analyzed by HPLC after labeling with 2-AA (Fig. 1b). A big peak (peak **E**) was observed at 53 min, which showed the same elution time with that of peak **C** observed in Fig. 1a. In addition, the peak showed the same MS and MS/MS profiles with those of peak **C** (Fig. 1e). In addition, the data also showed well matched results with those of biantennary glycan obtained from transferrin (data not shown). These results indicate that the peak at 53 min was clearly due to the glycan present in sera in free form. It should be noticed that some minor peaks were also observed from 25 min to 65 min.

3.2. Detailed analysis of free glycans in a serum sample

As described above, we found that free glycans are present in human serum samples. Fig. 2a shows the results on the detailed

Table 1
Summary of free glycans in human serum. (A) before neuraminidase digestion. (B) after neuraminidase digestion.

Peak no.	*m/z*	Monosaccharides composition	Content of free oligosaccharide (p mol/mL serum)
1	(A) 872 (2)	$Hex_4dHex_1HexNAc_4$-2AA	175
	(B) 872 (2)	$Hex_4dHex_1HexNAc_4$-2AA	
2	(A) 953 (2)	$Hex_5dHex_1HexNAc_4$-2AA	256
	(B) 953 (2)	$Hex_5dHex_1HexNAc_4$-2AA	
3, 4	(A) 794 (1)	$NeuAc_1Hex_1HexNAc_1$-2AA	264 (peak 3)
	(B) 503 (1)	$Hex_1HexNAc_1$-2AA	224 (peak 4)
5	(A) 1099 (2)	$NeuAc_1Hex_5dHex_1HexNAc_4$-2AA	235
	(B) 953 (2)	$Hex_5dHex_1HexNAc_4$-2AA	
6	(A) 1025 (2)	$NeuAc_1Hex_5HexNAc_4$-2AA	844
	(B) 880 (2)	$Hex_5HexNAc_4$-2AA	
7	(A) 1171 (2)	$NeuAc_2Hex_5HexNAc_4$-2AA	572
	(B) 880 (2)	$Hex_5HexNAc_4$-2AA	
8	(A) 1244 (2)	$NeuAc_2Hex_5dHex_1HexNAc_4$-2AA	642
	(B) 953 (2)	$Hex_5dHex_1HexNAc_4$-2AA	
9	(A) 1171 (2)	$NeuAc_2Hex_5HexNAc_4$-2AA	7620
	(B) 880 (2)	$Hex_5HexNAc_4$-2AA	
10	(A) 1070 (2)	$NeuAc_2Hex_5HexNAc_3$-2AA	235
	(B) 778 (2)	$Hex_5HexNAc_3$-2AA	
11-①	(A) 1048 (3)	$NeuAc_3Hex_6dHex_1HexNAc_5$-2AA	1206
	(B) 1136 (2)	$Hex_6dHex_1HexNAc_5$-2AA	(Total contents
11-②	(A) 999 (3)	$NeuAc_3Hex_6HexNAc_5$-2AA	for 11-① and 11-②)
	(B) 1062 (2)	$Hex_6HexNAc_5$-2AA	

dHex, deoxyhexose; Hex, hexose; HexNAc, N-acetyl hexose; NeuAc, N-acetylneuraminic acid.

profile of free glycans present in a serum sample (equivalent to 100 μL serum as the injected volume). Each peak was collected and their structures were confirmed by MS technique (Fig. 3 and Table 1). Most of the peaks are commonly found in transferrin and other commercially available samples, and their structures are easily confirmed. Disialylated biantennary glycan showing the molecular ion at *m/z* 1171 (peak **9**) as the doubly charged ion was the most abundant glycan as already shown in Fig. 1. The amount was determined to be 7620 pmol/mL of serum as calculated from the fluorescent intensity based on 2-AA residue. Structures of the minor peaks were also determined by MS techniques and comparison of the elution times with those reported previously [9]. At the earlier elution times (ca. 25 min), neutral mono- and di-galactosylated biantennary glycans (**1** and **2**) were observed. Mono-sialylated biantennary glycans with or without a fucose residue were observed at ca. 39 min (**5** and **6**). In addition, trisialo-triantennary glycans with or without a fucose residue were also observed at 63 min (**11**). Interestingly, we found a glycan having a structure of NeuAc-Gal-GalNAc-2AA which is probably due to mucin-type glycoproteins, although the amount of these glycans were only ca. 250 pmol/mL of serum (**3** and **4**). These peaks (**3** and **4**) were also assigned by comparison of the elution times with

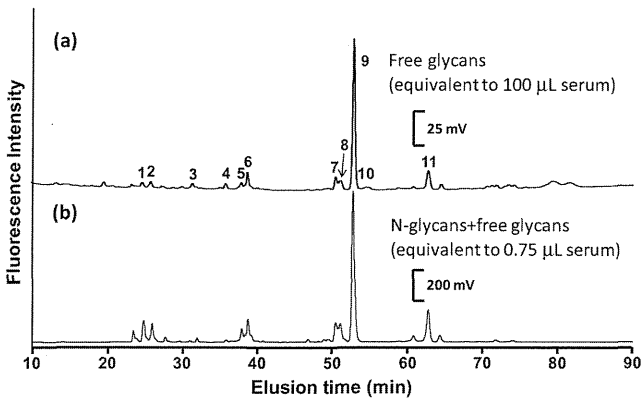

Fig. 2. HPLC analysis of (a) free glycans, and (b) total N-glycans in a human serum sample as examined after digestion with N-glycoamidase F. Analytical conditions are the same as those in Fig. 1.

those reported previously [10]. A characteristic glycan (**10**), disialo-biantennary glycan having one GlcNAc residue at the reducing end was also present in sera. We previously reported that this glycan was characteristically accumulated in cytosols of stomach tumor cells. The presence of this glycan may indicate that this characteristic glycan is leaked from some organs, although further studies are required [9]. According to the MS observations, peak **7** was assigned as disialo biantennary glycan by MS measurement. This indicates that peak **7** has different linkages of NeuAc to Gal with those of peak **9**. Because NeuAc mainly binds to Gal through α2-6 linkage in human [20], the glycan (**9**) is a typical disialo biantennary glycan which has NeuAcα2-6 linkages. And peak **7** is probably due to disialoglycan which has NeuAcα2-3 linkages. We also analyzed total N-glycans in a serum sample in order to consider the origin of free glycans in serum in detail. Fig. 2b shows the results on the profile of total N-glycans present in a serum sample (equivalent to 0.75 μL serum as the injected volume). As shown in Fig. 2b, the results are quite similar to those in Fig. 2a. It should be emphasized that high mannose-type glycans were not detected at all. This also indicates that these glycans are not due to cells from some organs but from sera, because high mannose-type glycans are major ones found in cytosol fractions through endoplasmic-reticulum associated protein degradation pathway [3].

Sturiale et al. studied glycosylation of transferrin in galactosemia patients in order to figure out hypoglycosylation with increased fucosylation and branching [21]. In the manuscript, they showed N-glycan profiles in a human serum sample (healthy volunteer) examined by MS technique after releasing N-glycans with N-glycoamidase F. The data showed quite similar profiles with those observed in the present study. Namely, Sturiale et al. reported that the ratios of triantennary glycan ($(Fuc)Gal_3GlcNAc_5Man_3NeuAc_3$), monosialo-biantennary glycan ($Gal_2GlcNAc_4Man_3NeuAc$) and disialo-fucosylated biantennary glycan ($FucGal_2GlcNAc_4Man_3NeuAc_2$) to the main glycan ($Gal_2GlcNAc_4Man_3NeuAc_2$) were 13.5, 9.4 and 6.5%, respectively. In the present study, the ratios of these glycans to the major glycan (**9**) were 15.8, 11.1 and 8.4%, respectively. These data clearly indicate that these glycans are possibly derived from serum glycoproteins containing transferrin during its circulation in bodies.

Free glycans found in the cytosol have only a single GlcNAc at their reducing termini [2], and this is due to the action of

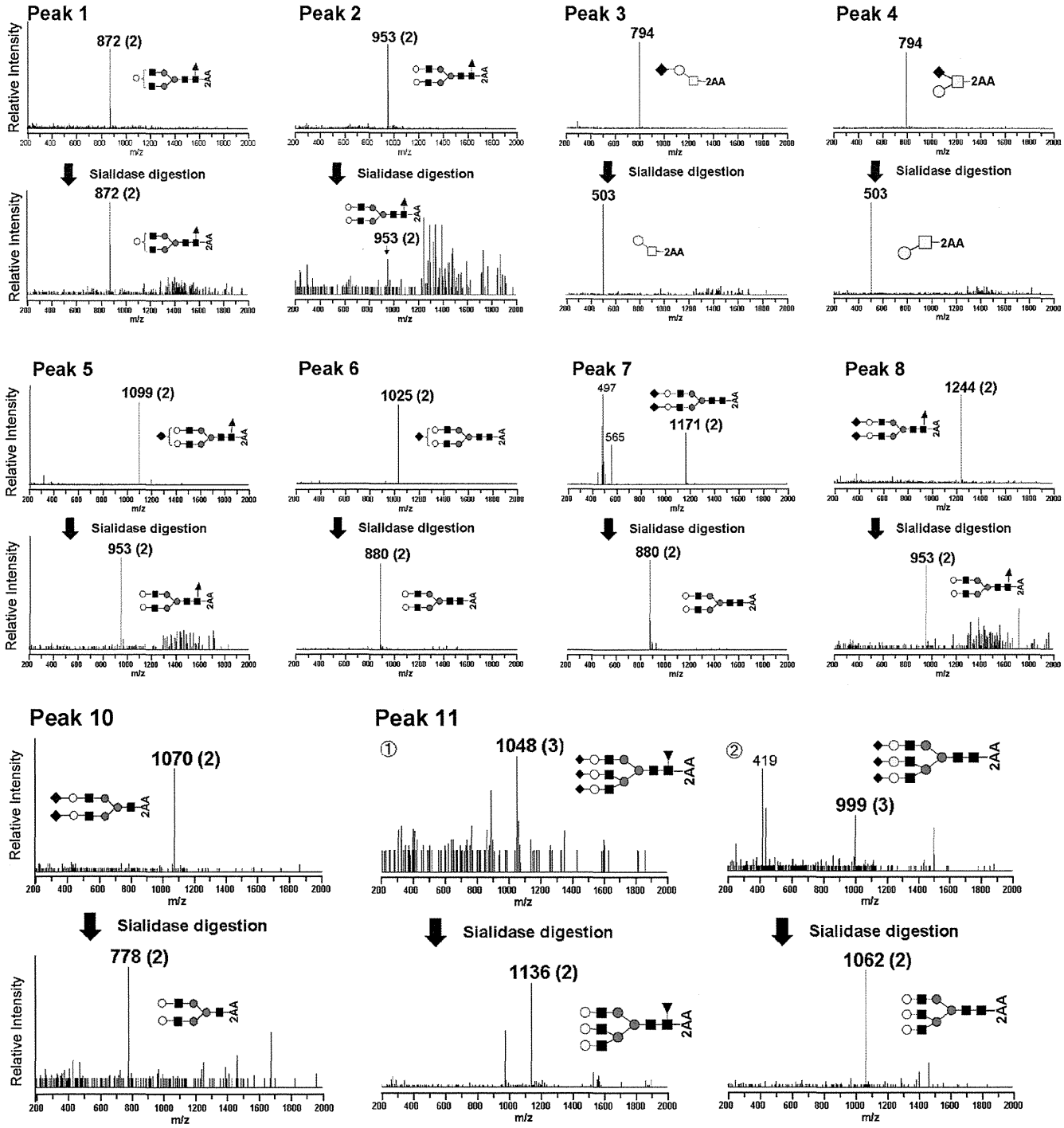

Fig. 3. ESI-IT-TOF mass spectra of peak 1–8, 10, 11 in Fig. 2. Symbols: triangles, fucose; others are the same as those in Fig. 1. Upper panels show the MS spectra of collected peaks. The collected peaks were digested with neuraminidase, and also analyzed by MS (lower panels).

the cytosolic ENGase (endo-β-N-acetylglucosaminidase) [22,23] or chitobiase [24]. It should be noted that most free glycans found in the present study bear N-acetylchitobiose structure other than peak **10**. Kimura et al. reported that free glycans were accumulated not only inside cells but also secreted to the extracellular space in rice cell culture [25,26]. In addition, they suggested that the extracellular acidic peptide N-glycanase was involved in accumulation of such glycans. We have to also consider the presence of free O-glycans (**3** and **4**), although the amounts of these glycans are quite small.

The mechanism of the presence/formation of free glycans in sera and the source of these glycans are not clear in the present study. However, it is quite interesting if these glycans are varied with physiological changes.

4. Conclusions

The present study demonstrates that free glycans exist in human serum. Most of the glycans were sialic acid-containing complex-type glycans. Of the glycans, disialo-biantennary glycan which does

not carry fucose residue is present most abundantly. And high mannose-type glycans were not detected at all. From these results, we suppose that these free glycans were due to glycoproteins in sera, although further studies are required.

References

[1] D. Kmiecik, V. Herman, C.J. Stoop, A.M. Mir, O. Labiau, A. Verbert, Glycobiology 5 (1995) 483.
[2] K. Yanagida, S. Natsuka, S. Hase, Glycobiology 16 (2006) 294.
[3] T. Suzuki, H. Park, W.J. Lennarz, FASEB J. 16 (2002) 635.
[4] I. Chantret, S.E. Moore, Glycobiology 18 (2008) 210.
[5] T. Suzuki, Y. Funakoshi, Glycoconj. J. 23 (2006) 291.
[6] D.J. Kelleher, R. Gilmore, Glycobiology 16 (2006) 47R.
[7] T. Suzuki, Semin Cell, Dev. Biol. 18 (2007) 762.
[8] R. Naka, S. Kamoda, A. Ishizuka, M. Kinoshita, K. Kakehi, J. Proteome Res. 5 (2006) 88.
[9] A. Ishizuka, Y. Hashimoto, R. Naka, M. Kinohita, K. Kakehi, J. Seino, Biochem. J. 413 (2008) 227.
[10] Y. Matsuno, K. Yamada, A. Tanabe, M. Kinoshita, S. Maruyama, Y. Osaka, T. Masuko, K. Kakehi, Anal. Biochem. 362 (2007) 245.
[11] K. Yamada, S. Hyodo, Y. Matsuno, M. Kinoshita, S. Maruyama, Y. Osaka, E. Casal, Y.C. Lee, K. Kakehi, Anal. Biochem. 371 (2007) 52.
[12] K. Yamada, M. Kinoshita, T. Hayakawa, S. Nakaya, K. Kakehi, J. Proteome Res. 8 (2009) 521.
[13] K. Yamada, S. Hyodo, M. Kinoshita, T. Hayakawa, K. Kakehi, Anal. Chem. 82 (2010) 7436.
[14] B. Winchester, Glycobiology 15 (2005) 1R.
[15] J.C. Michalski, J. Lemone, J.M. Wieruszeski, B. Fournet, J. Montreuil, G. Strecker, Eur. J. Biochem. 198 (1991) 521.
[16] G. Strecker, M.C. Peers, J.C. Michalski, T. Hondi-Assah, B. Fournet, G. Spik, J. Montreuil, J.P. Farriaux, P. Maroteaux, P. Durand, Eur. J. Biochem. 75 (1977) 391.
[17] J. van Pelt, K. Hard, J.P. Kamerking, J.F. Vliegenthart, A.J. Reuser, H. Galjaard, Biol. Chem. Hoppe-Seyler 370 (1989) 191.
[18] K. Ishii, M. Iwasaki, S. Inoue, P.T.M. Kenny, H. Komura, Y. Inoue, J. Biol. Chem. 264 (1989) 1623.
[19] M. Tajiri, C. Ohyama, Y. Wada, Glycobiology 18 (2008) 2.
[20] G. Weisshaar, J. Hiyama, A.G.C. Renwick, Glycobiology 1 (1991) 393.
[21] L. Sturiale, R. Barone, A. Fiumara, M. Perez, M. Zaffanello, G. Sorge, L. Pavone, S. Tortorelli, J.F. O'Brien, J. Jaeken, D. Garozzo, Glycobiology 15 (2005) 1268.
[22] T. Kato, K. Hatanaka, T. Mega, S. Hase, J. Biochem. 122 (1997) 1167.
[23] T. Suzuki, K. Yano, S. Sugimoto, K. Kitajima, W.J. Lennarz, S. Inoue, Y. Inoue, Y. Emori, Proc. Natl. Acad. Sci. U.S.A. 99 (2002) 9691.
[24] R. Cacan, C. Dengremont, O. Labiau, D. Kmiecik, A. Mir, A.M. Verbert, J. Biochem. 313 (1996) 597.
[25] Y. Kimura, S. Matsuo, J. Biochem. 127 (2000) 1013.
[26] M. Maeda, M. Kimura, Y. Kimura, J. Biochem. 148 (2010) 681.

BNIP3 Plays Crucial Roles in the Differentiation and Maintenance of Epidermal Keratinocytes

Mariko Moriyama[1,2,4], Hiroyuki Moriyama[1,4], Junki Uda[1], Akifumi Matsuyama[2], Masatake Osawa[3] and Takao Hayakawa[1]

Transcriptome analysis of the epidermis of *Hes1*$^{-/-}$ mouse revealed the direct relationship between Hes1 (hairy and enhancer of split-1) and BNIP3 (BCL2 and adenovirus E1B 19-kDa-interacting protein 3), a potent inducer of autophagy. Keratinocyte differentiation is going along with activation of lysosomal enzymes and organelle clearance, expecting the contribution of autophagy in this process. We found that BNIP3 was expressed in the suprabasal layer of the epidermis, where autophagosome formation is normally observed. Forced expression of BNIP3 in human primary epidermal keratinocytes (HPEKs) resulted in autophagy induction and keratinocyte differentiation, whereas knockdown of BNIP3 had the opposite effect. Intriguingly, addition of an autophagy inhibitor significantly suppressed the BNIP3-stimulated differentiation of keratinocytes, suggesting that BNIP3 plays a crucial role in keratinocyte differentiation by inducing autophagy. Furthermore, the number of dead cells increased in the human epidermal equivalent of BNIP3 knockdown keratinocytes, which suggests that BNIP3 is important for maintenance of skin epidermis. Interestingly, although UVB irradiation stimulated BNIP3 expression and cleavage of caspase3, suppression of UVB-induced BNIP3 expression led to further increase in cleaved caspase3 levels. This suggests that BNIP3 has a protective effect against UVB-induced apoptosis in keratinocytes. Overall, our data provide valuable insights into the role of BNIP3 in the differentiation and maintenance of epidermal keratinocytes.

Journal of Investigative Dermatology advance online publication, 6 February 2014; doi:10.1038/jid.2014.11

INTRODUCTION

The skin epidermis is a stratified epithelium. Stratification is a key process of epidermal development. During epidermal development, the single layer of basal cells undergoes asymmetric cell division to stratify, and produce committed suprabasal cells on the basal layer. These suprabasal cells are still immature and sustain several rounds of cell divisions to form fully stratified epithelia. Recent studies have identified numerous molecules involved in epidermal development, although how these molecules coordinate to induce proper stratification of the epidermis remains to be elucidated. Previously, by integrating both loss- and gain-of-function studies of Notch receptors and their downstream target Hes1 (hairy and enhancer of split-1), we demonstrated the multiple roles of Notch signaling in the regulation of suprabasal cells (Moriyama *et al.*, 2008). Notch signaling induces differentiation of suprabasal cells in a Hes1-independent manner, whereas Hes1 is required for maintenance of the immature status of suprabasal cells by preventing premature differentiation. In light of the critical role of Hes1 in the maintenance of spinous cells, exploration of the molecular targets of Hes1 in spinous layer cells may lead to the discovery of the molecules required for differentiation of spinous layer cells to granular layer cells. Because Hes1 is thought to be a transcriptional repressor (Ohtsuka *et al.*, 1999), loss of Hes1 is expected to cause aberrant upregulation of genes that are normally repressed in spinous layer cells. To identify these genes, we previously conducted comparative global transcript analysis using microarrays and found several candidates that may play a crucial role in regulating epidermal development (Moriyama *et al.*, 2008). One of the genes that was highly expressed was *BNIP3* (*BCL2 and adenovirus E1B 19-kDa-interacting protein 3*), an atypical pro-apoptotic BH3-only protein that induces cell death and autophagy (Zhang and Ney, 2009).

The molecular mechanism through which BNIP3 induces cell death is not well understood; however, it has been reported that BNIP3 protein is induced by hypoxia in some tumor cells and that the kinetics of this induction correlate with cell death (Sowter *et al.*, 2001). In contrast,

[1]*Pharmaceutical Research and Technology Institute, Kinki University, Higashi-Osaka, Osaka, Japan;* [2]*Platform for Realization of Regenerative Medicine, Foundation for Biomedical Research and Innovation, Kobe, Hyogo, Japan and* [3]*Division of Regeneration Technology, Gifu University School of Medicine, Gifu, Gifu, Japan*

[4]*These authors contributed equally to this work.*

Correspondence: Mariko Moriyama, Pharmaceutical Research and Technology Institute, Kinki University, Higashi-Osaka, Osaka 577-8502, Japan. E-mail: mariko@phar.kindai.ac.jp

Abbreviations: 3-MA, 3-methyladenine; BNIP3, BCL2 and adenovirus E1B 19-kDa-interacting protein 3; ChIP, chromatin immunoprecipitation; Hes1, hairy and enhancer of split-1; HPEK, human primary epidermal keratinocyte; Q-PCR, quantitative PCR

Received 18 July 2013; revised 10 December 2013; accepted 18 December 2013; accepted article preview online 8 January 2014

BNIP3-induced autophagy has been shown to protect HL-1 myocytes from cell death in an ischemia–reperfusion model (Hamacher-Brady *et al.*, 2007). Induction of autophagy by BNIP3 has a protective effect in some conditions, whereas in others it is associated with autophagic cell death. Recent evidence also suggests that BNIP3, through autophagy, is also required for the differentiation of chondrocytes under hypoxic conditions (Zhao *et al.*, 2012).

Autophagy was initially described based on its ultrastructural features of the double-membraned structures that surrounded the cytoplasm and organelles in cells, known as autophagosomes (Mizushima *et al.*, 2010). To date, only microtubule-associated protein light chain 3 (LC3), a mammalian homolog of yeast Atg8, is known to be expressed in autophagosomes and, therefore, it serves as a widely used marker for autophagosomes (Kabeya *et al.*, 2000; Mizushima *et al.*, 2004). Autophagy is an evolutionarily conserved catabolic program that is activated in response to starvation or changing nutrient conditions. Recently, autophagy was shown to be involved in differentiation of multiple cell types, including erythrocytes, lymphocytes, adipocyte, neuron, and chondrocyte (Srinivas *et al.*, 2009; Mizushima and Levine, 2010).

Epidermal cornification, the process of terminal keratinocyte differentiation, requires programmed cell death in a similar but different pathway from apoptosis (Lippens *et al.*, 2005). Cornification is also accompanied by activation of lysosomal enzymes and organelle clearance. Moreover, some researchers have reported that autophagy may play a role in epidermal differentiation (Haruna *et al.*, 2008; Aymard *et al.*, 2011; Chatterjea *et al.*, 2011). Therefore, it is likely that BNIP3 is involved in cornification through cell death or autophagy.

In this study, transcriptome analysis of *Hes1*$^{-/-}$ mouse epidermis revealed that Hes1 could directly suppress BNIP3 expression in epidermal keratinocytes. We also found that BNIP3 was expressed in the suprabasal layer of the human skin epidermis, where autophagosome formation was observed. BNIP3 was also sufficient to promote cornification through induction of autophagy. Finally, we found that BNIP3 had a protective effect against UVB-induced apoptosis in keratinocytes *in vitro*. Our data thus indicate that BNIP3, an inducer of autophagy, is involved in the terminal differentiation and maintenance of epidermal keratinocytes.

RESULTS

Hes1 directly represses BNIP3 expression in epidermal cells and keratinocytes

We previously performed a microarray analysis with epidermal RNAs isolated from wild-type and *Hes1*$^{-/-}$ mice (Moriyama *et al.*, 2008) and found that BNIP3 was preferentially overexpressed in *Hes1*$^{-/-}$ epidermis. The upregulation of *Bnip3* in the *Hes1*$^{-/-}$ epidermis was confirmed by quantitative PCR (Q-PCR) and immunofluorescent staining (Figure 1a and b). As Hes1 is thought to be a transcriptional repressor (Ishibashi *et al.*, 1994), it might play a repressive role in the regulation of BNIP3 expression. In accordance with this hypothesis, BNIP3 expression in *Hes1*$^{-/-}$ epidermis at embryonic day 15.5 was observed in the suprabasal layers (Figure 1b), where Hes1 has been reported to be expressed in wild-type epidermis at the same age (Blanpain *et al.*, 2006; Moriyama *et al.*, 2008). To confirm whether Hes1 suppresses BNIP3 expression, an adenoviral vector expressing Hes1 was used to infect human primary epidermal keratinocytes (HPEKs) and, subsequently, the expression level of BNIP3 was quantified by Q-PCR and western blot analysis. The BNIP3 protein was detected as multiple bands between 22 and 30 kD as previously reported (Vengellur and LaPres, 2004; Walls *et al.*, 2009; Mellor *et al.*, 2010; Sassone *et al.*, 2010). We found that Hes1 induced a substantial reduction of BNIP3 expression in HPEKs at the mRNA and protein levels (Figure 1c and d), demonstrating that Hes1 is involved in the repression of BNIP3. To determine whether Hes1 directly regulates *BNIP3* expression, we performed chromatin immunoprecipitation (ChIP) assays. We identified at least 5 Hes1 consensus binding sites 1 kb upstream of the transcription initiation site of the human *BNIP3* gene, and subsequent Q-PCR analysis revealed that a DNA fragment located at -247 to -87 was slightly amplified from crosslinked chromatin isolated by Hes1 immunoprecipitation (Figure 1e). We also found an additional site between -212 and $+22$ that was strongly amplified. These data clearly show that Hes1 specifically binds to the promoter region of *BNIP3* and directly suppresses its expression.

BNIP3 is expressed in the granular layer of the epidermis, where autophagosome formation is observed

To determine the BNIP3 expression profile in the epidermis, we performed immunofluorescent staining in human skin epidermal equivalent. BNIP3 was expressed in the granular layer of epidermal equivalent 18 days (Figure 2a and b) or 24 days (Figure 2c and d) after exposure at the air–liquid interface. BNIP3 expression in the granular layer was also observed in the normal human skin epidermis (Figure 2g and h). Recent reports show that BNIP3 is expressed in mitochondria and that it induces autophagy (Quinsay *et al.*, 2010). In addition, some researchers have reported that autophagy may play a role in epidermal differentiation (Haruna *et al.*, 2008; Aymard *et al.*, 2011; Chatterjea *et al.*, 2011). We therefore investigated whether autophagy occurred in the epidermis, especially in the granular layers. To quantitate the level of autophagy, cytosol to membrane translocation of the autophagy marker EGFP-LC3 (Kabeya *et al.*, 2000) was monitored in a human skin equivalent model (Mizushima *et al.*, 2004). When autophagy is active, autophagosomes containing EGFP-LC3 are visible as fluorescent puncta (Kabeya *et al.*, 2000). As expected, EGFP-LC3 puncta were observed in the granular layers of the epidermal equivalent (Figure 2e). Moreover, endogenous LC3 dots were observed in the granular layers of normal human skin epidermis (Figure 2f). These data suggested that BNIP3 might be involved in the induction of autophagy in the granular layer of the epidermis.

BNIP3 is required for terminal differentiation of keratinocyte by induction of autophagy *in vitro*

To investigate the involvement of BNIP3 in the induction of autophagy, we transduced HPEKs stably expressing EGFP-LC3

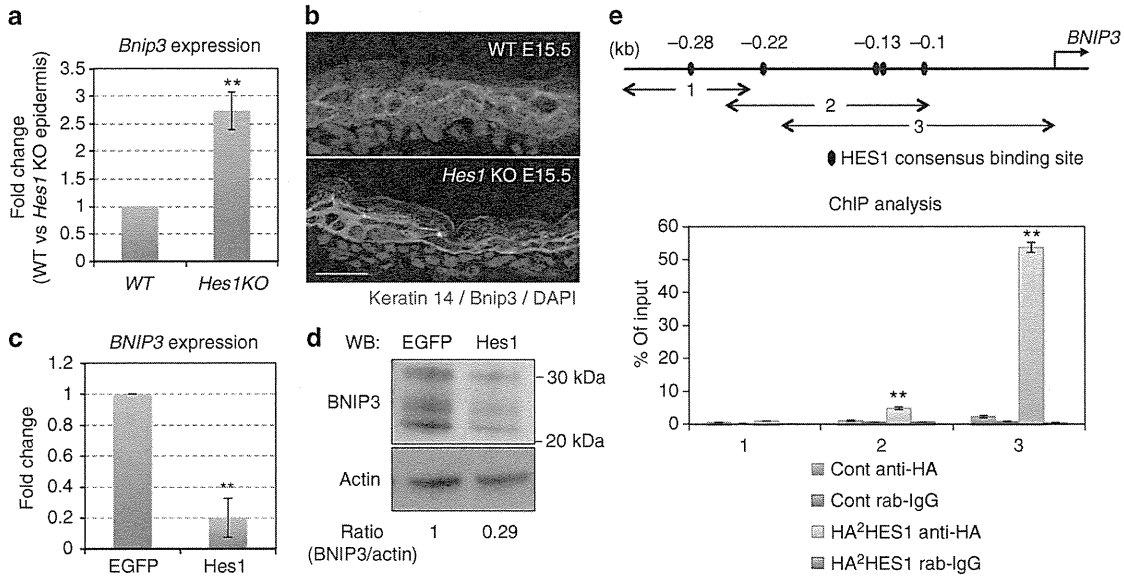

Figure 1. BNIP3 (BCL2 and adenovirus E1B 19-kDa-interacting protein 3) is directly suppressed by HES1(hairy and enhancer of split-1). (**a**) Quantitative PCR (Q-PCR) analysis of *Bnip3* expression in dorsal skin epidermis from either wild-type (WT) or *Hes1* knockout (KO) embryo (embryonic day 14.5 (E14.5)). (**b**) Immunofluorescent analysis of Bnip3 expression in dorsal skin epidermis from either WT or *Hes1* KO embryo (E15.5). Keratin 14 staining is shown in green and Bnip3 staining is shown in red. The blue signals indicate nuclear staining. Scale bars = 20 μm. (**c**) Q-PCR and (**d**) western blot analysis of BNIP3 expression in human primary epidermal keratinocyte (HPEK) cells infected with adenoviruses expressing enhanced green fluorescent protein (EGFP) or Hes1. (**c**) Each expression value was calculated with the ΔΔCt method using *UBE2D2* as an internal control. (**d**) Numbers below blots indicate relative band intensities as determined by ImageJ software. (**e**) Specific binding of Hes1 to the *BNIP3* promoter. HPEK cells were infected with adenoviral constructs expressing hemagglutinin (HA)-tagged Hes1, and processed for chromatin immunoprecipitation (ChIP) with an anti-HA antibody and normal rabbit immunoglobulin G (Cont rab-IgG) as a nonimmune control. Q-PCR amplification of the region of the *BNIP3* gene described in the indicated map (upper panel; nucleotides −360 to −244 (1); nucleotides −247 to −87 (2); −212 to +22 (3)) was also performed. The amount of precipitated DNA was calculated relative to the total input chromatin. All the data represent the average of three independent experiments ± SD. $^{**}P<0.01$.

with a BNIP3 adenoviral vector. BNIP3 expression was found to be sufficient to trigger the formation of EGFP-LC3 puncta that was significantly reduced by addition of 3-methyladenine (3-MA), an inhibitor of autophagy (Figure 3a and b). On the other hand, BNIP3 knockdown markedly decreased the punctuate distribution of EGFP-LC3 in differentiated HPEKs (Figure 3c and d). Furthermore, flow cytometry analysis using a green fluorescent probe used to specifically detect autophagy (Cyto-ID autophagy detection dye) (Chan *et al.*, 2012) also showed that BNIP3 was required for the autophagy induction (Figure 3c and f). These data indicate that BNIP3 is involved in the induction of autophagy in HPEKs. Intriguingly, these data also confirm the previous finding that autophagosome induction is accompanied by keratinocyte differentiation (Haruna *et al.*, 2008). We observed that the number of mitochondria was decreased in the granular layers, where BNIP3 expression and autophagosome formation was observed (Figure 4a). In addition, mitochondria were significantly decreased in the differentiated HPEKs *in vitro* (Figure 4b). Colocalizations of mitochondria and EGFP-LC3 dot were observed only in the differentiating keratinocytes (Figure 4c), suggesting the contribution of autophagy in the decrease of mitochondria. BNIP3 expression was also correlated with decreased mitochondria in HPEKs, whereas addition of 3-MA restored mitochondrial numbers (Figure 4d). Furthermore, we also observed colocalization of mitochondria and EGFP-LC3 dot in BNIP3-overexpressing HPEKs (Figure 4e). These data indicated that mitochondria were removed by BNIP3-induced autophagy. Next, we investigated the involvement of BNIP3 in the differentiation of epidermal keratinocytes. Western blot analysis and immunofluorescent staining revealed that BNIP3 expression increased during differentiation (Figure 5a and b). Knockdown of BNIP3 significantly suppressed keratinocyte differentiation when the cells were treated with differentiation medium (Figure 5c and d), indicating that BNIP3 is required for terminal differentiation of keratinocyte. On the other hand, forced expression of BNIP3 in HPEKs markedly stimulated loricrin expression (Figure 5e and f). To determine whether BNIP3-dependent keratinocyte differentiation was induced by autophagy, 3-MA was added to the cells transduced with BNIP3. As shown in Figure 5e and f, 3-MA notably abolished the keratinocyte differentiation induced by BNIP3, suggesting that BNIP3 is required for terminal differentiation of keratinocyte by induction of autophagy.

BNIP3 maintains epidermal keratinocytes

To further determine the roles of BNIP3 in epidermal differentiation, the human skin epidermal equivalent was reconstituted from HPEKs stably expressing a BNIP3 RNA interference (RNAi). Unfortunately, we did not observe drastic differentiation defects; however, we unexpectedly discovered